Molecular Therapy
Original Article

Optimization of Retinal Gene Therapy for X-Linked Retinitis Pigmentosa Due to *RPGR* Mutations

William A. Beltran,[1,7] Artur V. Cideciyan,[2,7] Shannon E. Boye,[3] Guo-Jie Ye,[4] Simone Iwabe,[1] Valerie L. Dufour,[1] Luis Felipe Marinho,[1] Malgorzata Swider,[2] Mychajlo S. Kosyk,[2] Jin Sha,[2] Sanford L. Boye,[3] James J. Peterson,[3] C. Douglas Witherspoon,[5] John J. Alexander,[6] Gui-Shuang Ying,[2] Mark S. Shearman,[4] Jeffrey D. Chulay,[4] William W. Hauswirth,[3] Paul D. Gamlin,[5] Samuel G. Jacobson,[2] and Gustavo D. Aguirre[1]

[1]Division of Experimental Retinal Therapies, Department of Clinical Studies, School of Veterinary Medicine, University of Pennsylvania, Philadelphia, PA 19014, USA; [2]Scheie Eye Institute, Department of Ophthalmology, Perelman School of Medicine, University of Pennsylvania, Philadelphia, PA 19104, USA; [3]Department of Ophthalmology, College of Medicine, University of Florida, Gainesville, FL 32610, USA; [4]Applied Genetic Technologies Corporation, Alachua, FL 32615, USA; [5]Department of Ophthalmology, School of Medicine, University of Alabama at Birmingham, Birmingham, AL 35294, USA; [6]Department of Human Genetics, School of Medicine, Emory University, Atlanta, GA 30303, USA

X-linked retinitis pigmentosa (XLRP) caused by mutations in the *RPGR* gene is an early onset and severe cause of blindness. Successful proof-of-concept studies in a canine model have recently shown that development of a corrective gene therapy for *RPGR*-XLRP may now be an attainable goal. In preparation for a future clinical trial, we have here optimized the therapeutic AAV vector construct by showing that GRK1 (rather than IRBP) is a more efficient promoter for targeting gene expression to both rods and cones in non-human primates. Two transgenes were used in *RPGR* mutant (XLPRA2) dogs under the control of the GRK1 promoter. First was the previously developed stabilized human *RPGR* (*hRPGRstb*). Second was a new full-length stabilized and codon-optimized human *RPGR* (*hRPGRco*). Long-term (>2 years) studies with an AAV2/5 vector carrying *hRPGRstb* under control of the GRK1 promoter showed rescue of rods and cones from degeneration and retention of vision. Shorter term (3 months) studies demonstrated comparable preservation of photoreceptors in canine eyes treated with an AAV2/5 vector carrying either transgene under the control of the GRK1 promoter. These results provide the critical molecular components (GRK1 promoter, *hRPGRco* transgene) to now construct a therapeutic viral vector optimized for *RPGR*-XLRP patients.

INTRODUCTION

Inherited retinal degenerations (RDs) are a heterogeneous group of blinding diseases with autosomal recessive, autosomal dominant, and X-linked forms.[1] RDs remain incurable, but gene therapy approaches are showing promise.[2–4] One of the most common molecular forms of RD is X-linked retinitis pigmentosa (XLRP), which is caused by mutations in the retinitis pigmentosa GTPase regulator (*RPGR*) gene.[5–10] The great majority of the patients affected with *RPGR*-XLRP carry mutations in the ORF15 exon. In dogs, naturally occurring frameshift mutations in the ORF15 exon of canine *RPGR* result in RD.[11] Initial gene therapy experiments with an AAV2/5 vector carrying a stabilized human *RPGR* (*hRPGRstb*) cDNA[12] showed proof of concept of rescue of photoreceptors from progressive degeneration using either a human interphotoreceptor retinoid-binding protein (IRBP) promoter[13] or a human rhodopsin kinase (GRK1)[14] promoter.[15,16] Further experiments performed with the IRBP promoter showed that the rescue effect was substantial and long-lasting, and efficacy was demonstrable, not only when intervention was timed at early stages of disease, but also with injections performed at later stages of disease.[17]

On the path to clinical translation, we first evaluated the comparative transduction efficacy of the IRBP and GRK1 promoters with GFP in non-human primates (NHPs). The results suggested that GRK1 promotes expression in primate cone photoreceptors with greater efficiency compared to IRBP. Therefore, further studies were designed to evaluate the efficacy and durability of AAV2/5 vectors containing the GRK1 promoter in *RPGR* mutant (XLPRA2) dogs using several titers. In addition, the potency of the *hRPGRstb* transgene, which is 39 bp shorter than the published DNA sequence due to multiple in-frame 3-nt deletions and has 65-nt changes that cause 28 amino acid mutations, was compared to that of a newly developed codon-optimized full-length human *hRPGR* cDNA (*hRPGRco*) that codes for an RPGR protein identical to the natural RPGR ORF15 protein.

Received 12 February 2017; accepted 5 May 2017;
http://dx.doi.org/10.1016/j.ymthe.2017.05.004.

[7]These authors contributed equally to this work.

Correspondence: William A. Beltran, School of Veterinary Medicine, University of Pennsylvania, 3900 Delancey Street, Philadelphia, PA 19104, USA.
E-mail: wbeltran@vet.upenn.edu

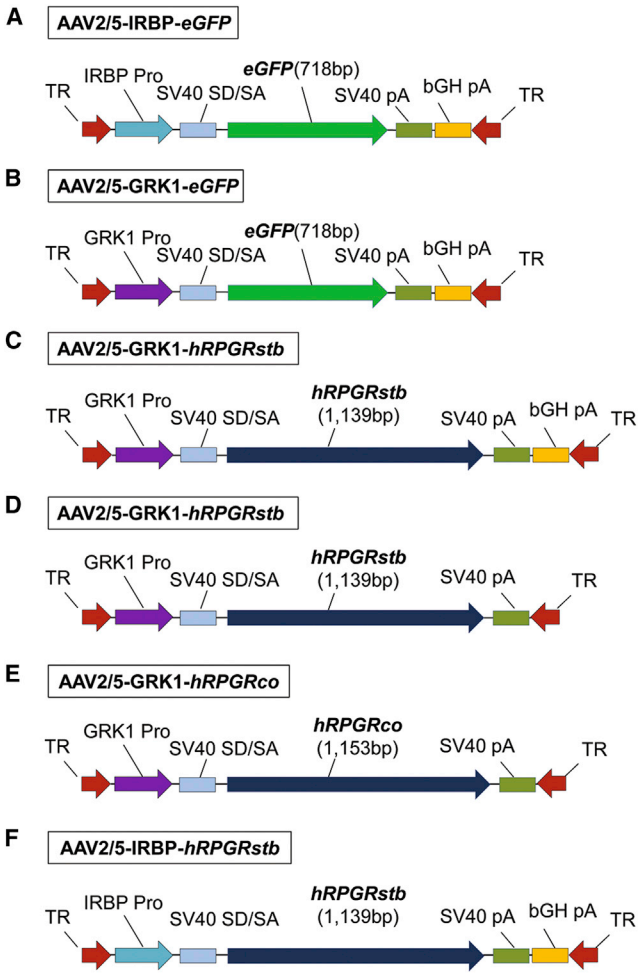

Figure 1. Recombinant AAV Vectors Used in the Study

(A and B) rAAV vectors containing a human IRBP promoter (IRBP Pro) or human GRK1 promoter (GRK1 Pro) driving expression of a humanized enhanced GFP reporter gene (*eGFP*). (C–F) rAAV vectors containing a human GRK1 promoter or human IRBP promoter driving expression of different versions of the human *RPGR* cDNA. *hRPGRstb* and *hRPGRco* are two versions of human RPGR$^{exon1\text{-}ORF15}$, with nucleotide sequence differences in exon ORF15 described in Figure S5. With the exception of bGH pA not being included in constructs (D) and (E), all other elements (SV40 SD/SA and poly A signals) within these constructs are identical. TR, AAV2-inverted terminal repeats; SV40 SD/SA, simian virus 40 splice donor/splice acceptor element; SV40 pA, simian virus 40 polyadenylation signal; bGH pA, bovine growth hormone polyadenylation signal.

RESULTS

Selection of Optimal Promoter for Transgene Expression in Rods and Cones of NHPs

Expression of GFP resulting from subretinal delivery of 50–100 μL of two AAV2/5 vector constructs (Figures 1A and 1B) at two dose range concentrations was examined ~8–10 weeks after injection in a total of eight eyes of two closely related macaque NHP species (Table S1). With a higher vector concentration (1–1.5 × 10^{12} vg/mL), in-life fluorescence imaging demonstrated GFP expression in central (Figures 2A and 2C) and peripheral (Figures 2B and 2D) retinal locations with both IRBP (Figures 2A and 2B) and GRK1 (Figures 2C and 2D) promoters. However, the foveo-macular region exhibited GFP fluorescence only after injection with AAV2/5-GRK1-e*GFP* (Figure 2C), but not with AAV2/5-IRBP-e*GFP* (Figure 2A). To identify the retinal cell origins of the fluorescence observed in life, morphological sections were performed in all eyes. GFP expression was not observed in foveal cone photoreceptors following injection with AAV2/5-IRBP-e*GFP* (Figure 2A). Images taken within, immediately temporal, and immediately nasal to the approximate foveal pit (Figures 2A1–2A3) revealed GFP expression outside the fovea concomitant with the appearance of rod photoreceptors (Figures 2A1 and 2A3). High-magnification images taken in the rod-containing central retina revealed GFP expression was excluded from cone-arrestin-positive cells and was thus restricted to rods (Figures 2A4–2A6). In the extra-macular retina, GFP expression was also restricted to rod photoreceptors (Figures 2B1–2B3), as evidenced by its lack of expression in cone-arrestin-positive cells. At a lower concentration (3 × 10^{11} vg/mL), GFP expression in foveal (Figure S1) and peripheral (data not shown) cones was also not detected. Both NHP subjects (080113 and 090365) had low (1:40) neutralizing antibody titers directed against AAV5 capsid prior to subretinal injection.

Injections of AAV2/5 containing the GRK1 promoter at high concentration (1.0 × 10^{12} vg/mL) led to GFP expression in foveal cones (Figures 2C1–2C3), and peripheral cones and rods (Figures 2D1–2D3). At a lower concentration (1.5 × 10^{11} vg/mL), GRK1-mediated GFP expression was restricted to rod photoreceptors (Figure S1). Both NHP subjects (AV136 and AT459) exhibited no detectable (titers <1:10) neutralizing antibodies to AAV5 capsid prior to subretinal injection.

Taken together, these results show that the IRBP promoter drives transgene expression exclusively in rod photoreceptors of NHPs at both 1 × 10^{12} vg/mL and 3 × 10^{11} vg/mL. Consistent with our previous findings,[18] the GRK1 promoter is active in both rod and cone photoreceptors near 1 × 10^{12} vg/mL. Consequently, the GRK1 promoter was incorporated into therapeutic vectors utilized in subsequent studies.

Efficacy of GRK1 Promoter in Early- and Mid-stage Canine Disease

AAV2/5-GRK1-*hRPGRstb* (Figure 1C) was used to determine the dose-response function and stability of treatment when administered at different stages of the disease. *RPGR* mutant eyes (n = 4) were injected with AAV2/5-GRK1-*hRPGRstb* at early-stage disease (5 weeks of age) with titers of 1.5 × 10^{11} and 1.5 × 10^{12} vg/mL (volume: 70−100 μL) and followed long term with non-invasive retinal imaging (Table S2). Early-stage disease is characterized by marked structural abnormalities of the photoreceptors, with no significant loss of the outer nuclear layer (ONL).[19] When evaluated at 2 years of age, ONL thickness topography showed a qualitatively preserved region within the treatment boundary in all eyes (Figure 3B). Quantitative results of ONL thickness at specific loci sampled across the treatment

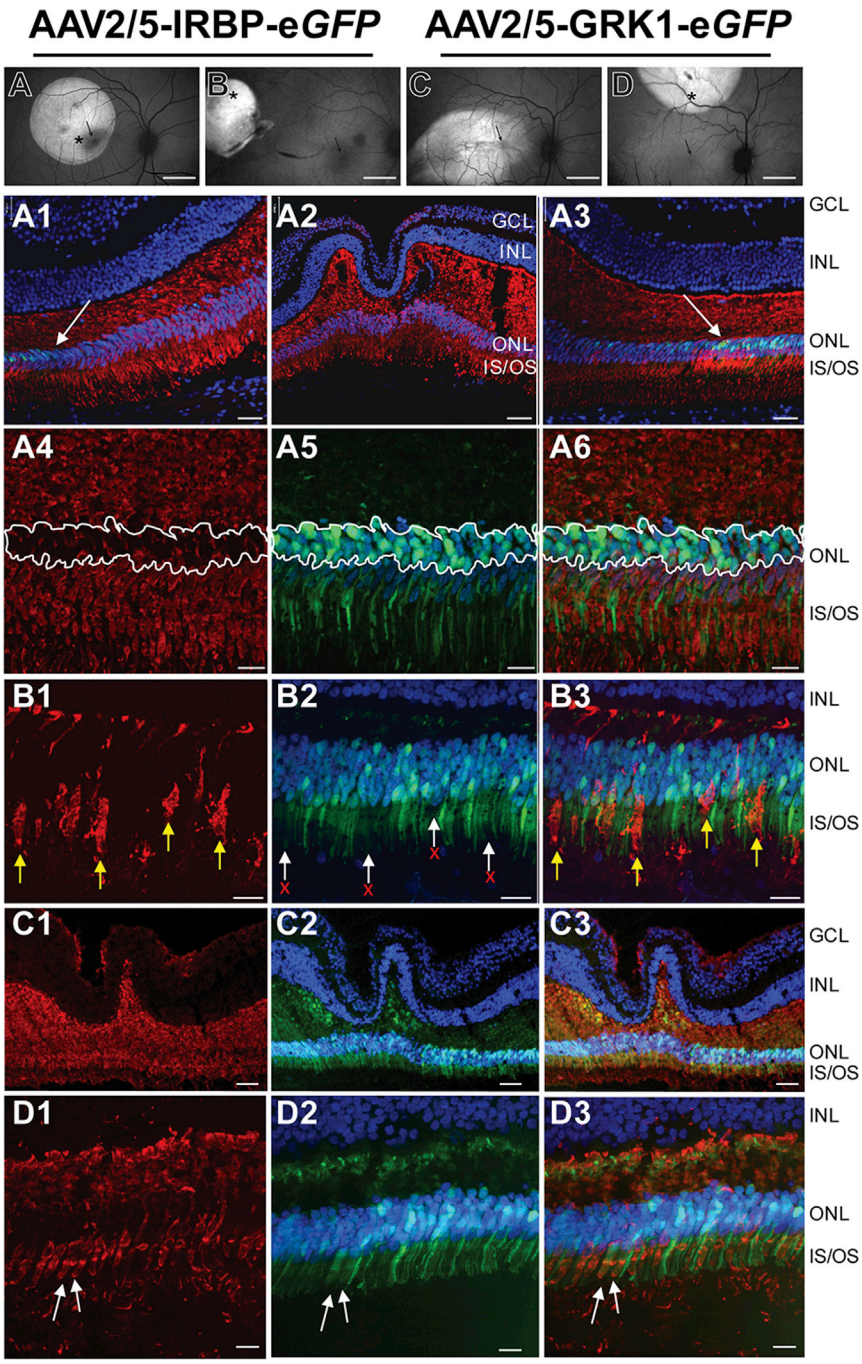

Figure 2. GFP Expression in Macaque Photoreceptors 8 Weeks Post-subretinal Injection with High Titers of AAV2/5 Using IRBP or GRK1 Promoters

(A) En face cSLO fundus image (displayed as equivalent right eye) showing GFP fluorescence in the central left retina of NHP #090365 treated with 100 μL of AAV2/5-IRBP-e*GFP* at 1 × 10^{12} vg/mL. Black arrow, fovea; asterisk, approximate location of immunolabeling images A4–A6. Retinal cross sections temporal to (A1), approximately within (A2), and nasal to (A3) the foveal pit, immunostained for cone arrestin (red) and counterstained with DAPI (blue) reveal a lack of rAAV2/5-IRBP-mediated GFP expression in central cones. White arrows in panels (A1) and (A3) delineate the eccentricity (~1,000 μm) from the fovea at which IRBP-driven GFP expression limited to rods is observed. High-magnification images in this region (A4–A6) reveal the location of rod cell bodies (outlined with white line) that lack cone arrestin labeling (A4). GFP expression is restricted to these cone arrestin-negative cells (A5 and A6). (B) En face cSLO fundus image showing GFP fluorescence in the peripheral right retina of NHP #090365 treated with 100 μL of AAV2/5-IRBP-e*GFP* at 1 × 10^{12} vg/mL. Black arrow, fovea; asterisk, approximate location of immunolabeling images B1–B3. rAAV2/5-IRBP-mediated GFP expression is found in rod, but not cone photoreceptors, as evidenced by a lack of GFP expression (white arrows, red Xs in panel B2) in cone-arrestin-positive cells (yellow arrows, panels B1 and B3). En face cSLO fundus image showing GFP fluorescence in the central right (C) and peripheral left (displayed as equivalent right eye) (D) retinas of NHP #AV136 treated with 90–100 μL of AAV2/5-GRK1-e*GFP* at 1 × 10^{12} vg/mL. Black arrow, fovea; asterisk, approximate location of immunolabeling images D1–D3. Immunolabeling in retinal cross sections reveal AAV2/5-GRK1-mediated GFP expression in central cones (C1–C3), peripheral cones (white arrows in D1–D3) and rods (D1–D3). Scale bars, 10° (A–D), 100 μm (A2 and C1–C3), 33 μm (A1 and A3), and 17 μm (A4–A6, B1–B3, and D1–D3).

boundary (Figure S2A) showed significantly greater retention of ONL thickness in AAV-treated loci compared to surrounding untreated loci (Figure 3D, lanes d and e). Untreated regions were 0.8 log reduced compared to wild-type (WT) controls, and this was consistent with the natural history of disease.[17] The treatment effect with the 1.5 × 10^{11} vg/mL titer averaged 0.29 log of preservation within the treated regions compared to the untreated regions at 2 years. With the higher 1.5 × 10^{12} vg/mL titer, there was 0.68 log of preservation, with an ONL thickness within the treated region approaching WT normal control levels.

Another cohort of *RPGR* mutant eyes (n = 12) was injected with AAV2/5-GRK1-*hRPGRstb* (Figure 1C) at mid-stage disease (12 weeks of age; ~40% loss of photoreceptors) with either control balanced salt solution (BSS) or vectors at titers of 1.5 × 10^{11} and 1.5 × 10^{12} vg/mL and followed long term (Table S2). When evaluated at 2 years of age, eyes injected with BSS showed no detectable differences of ONL thickness within the treated region compared to surrounding regions qualitatively (Figure 3C, left) or quantitatively (Figure 3D, lane f; Figure S2B). All regions were 1 log reduced compared to WT, consistent with the natural history of this disease.[17] With both titers of AAV2/5-GRK1-*hRPGRstb* vector, however, all eyes showed relatively

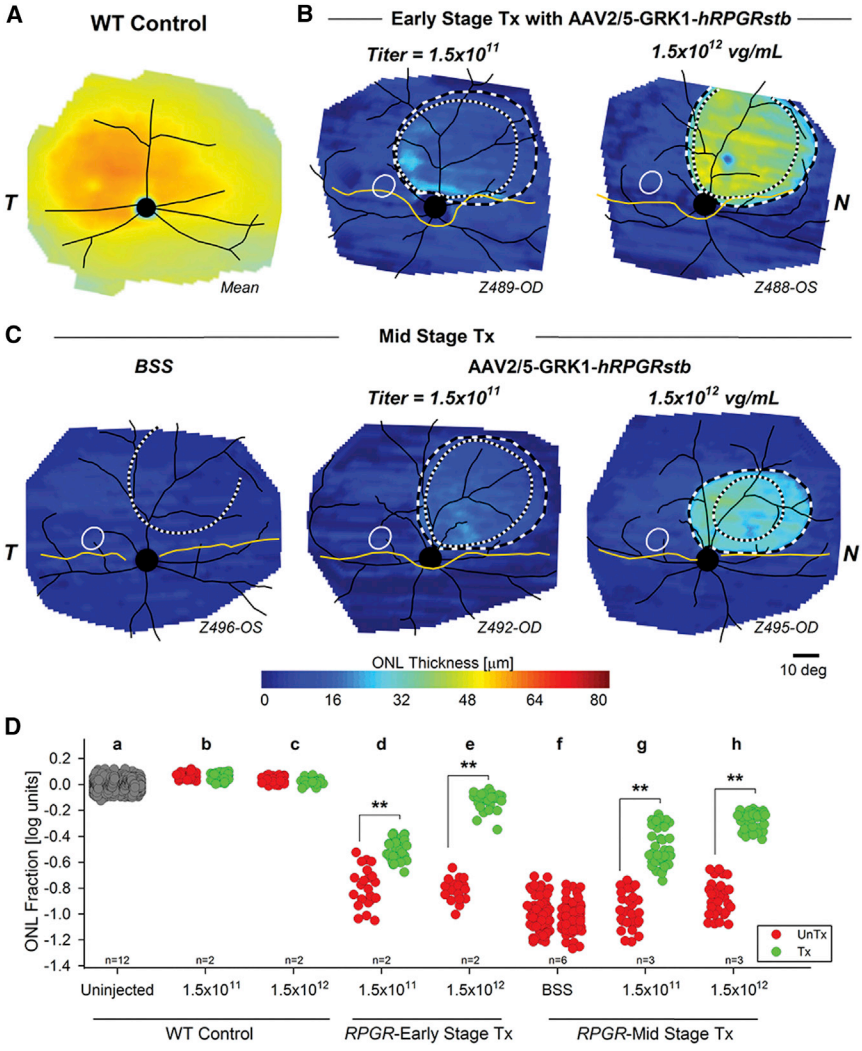

Figure 3. Dose Response Function and Long-Term Stability after Gene Therapy Intervention at Early- and Mid-stages of RPGR Disease

(A–C) WT control ONL thickness topography (A) compared to injected *RPGR* mutant (B and C) dogs. WT control map is the mean of 12 eyes (age 16–198 weeks; mean = 56 weeks). *RPGR* mutant maps are representatives from a cohort of 16 eyes injected subretinally with BSS control or two titers of AAV2/5-GRK1-*hRPGRstb* at early- (B) (5 weeks) or mid-stage (C) (12 weeks) disease and imaged at age 102–106 weeks. Treatment boundaries are based on fundus photographs of the bleb taken at the time of the injection (dotted lines), and, if visible, demarcations apparent on infrared imaging at the time of scanning (dashed lines). All eyes shown as equivalent right eyes with optic nerve and major blood vessels (black), tapetum boundary (yellow), and fovea-like region (white ellipse) overlaid for ease of comparison. T, temporal; N, nasal retina. Z489-OD and similar labels designate the individual animal and eye. (D) Difference of ONL thickness from mean control (ONL fraction in $\log_{10}$ units) at individual retinal locations in uninjected and injected WT control and *RPGR* mutant eyes. For each grouping of injected eyes (lanes b–h), the retinal loci outside the largest treatment boundary are shown on the left of the lane, and loci inside the boundary are shown on the right. Colors differentiate exposure to vector (green, Tx) versus BSS or no exposure (red, UnTx). Uninjected WT control eyes are shown with gray. **$p < 0.05$, t test. Numbers of eyes contributing to each lane are shown.

preserved ONL thickness qualitatively (Figure 3C, middle and right) and significant treatment effects quantitatively (Figure 3D, lanes g and h; Figure S2B). The average treatment effect at 2 years was 0.48 log of preservation for 1.5×10^{11} vg/mL and 0.60 log of preservation for 1.5×10^{12} vg/mL titer.

To evaluate the short-term safety of the AAV2/5-GRK1-*hRPGRstb* construct (Figure 1C), WT control eyes (n = 2) were injected with the vector at titers of 1.5×10^{11} or 1.5×10^{12} vg/mL at 14 weeks of age and evaluated clinically and by in vivo retinal imaging at 27 weeks (Table S2). No ophthalmic alterations were seen, and normal retinal lamination in the treated region was preserved. To evaluate the long-term safety of the AAV2/5-GRK1-*hRPGRstb* construct (Figure 1C), WT control eyes (n = 4) were injected with the vector at titers of 1.5×10^{11} or 1.5×10^{12} vg/mL at 5 weeks of age and followed long term (Table S2). At 102 weeks of age, there were neither detectable ocular adverse effects nor differences in terms of ONL thickness between injected regions and surrounding uninjected regions at either titer (Figure 3D, lanes b and c). To further assess the long-term safety of AAV2/5-GRK1-*hRPGRstb*, electroretinograms (ERGs) were performed in both eyes of one of the WT dogs injected at 5 weeks of age with the two titers. At 128 weeks of age, there were no differences or alterations in ERG amplitudes and traces, and these were similar to that of uninjected WT eyes (Figure S3).

Retinal and Visual Function Consequences of Treatment at Mid-stage Disease

Retinal function by ERG of *RPGR* mutant eyes injected at mid-stage disease (12 weeks) with AAV2/5-GRK1-*hRPGRstb* (Figure 1C) at 1.5×10^{11} (n = 3) and 1.5×10^{12} vg/mL (n = 3) titers was compared at 103 weeks of age to that of the BSS-injected contralateral eyes. All eyes were injected with a similar volume (150 µL) in the central supero-nasal retinal quadrant, which resulted in subretinal blebs of similar sizes in all eyes, with the exception of Z495-OD. In this eye, injected with the higher titer (1.5×10^{12} vg/mL), a smaller bleb (Figure 3C) was possibly due to partial reflux into the vitreous. ERG analyses of eyes injected with 1.5×10^{11} vg/mL showed improved rod function in one out of three retinas (data not shown), but a positive rescue of cone function in three out of three retinas when compared to the BSS-injected contralateral eyes (Figures 4A and 4B). The mean

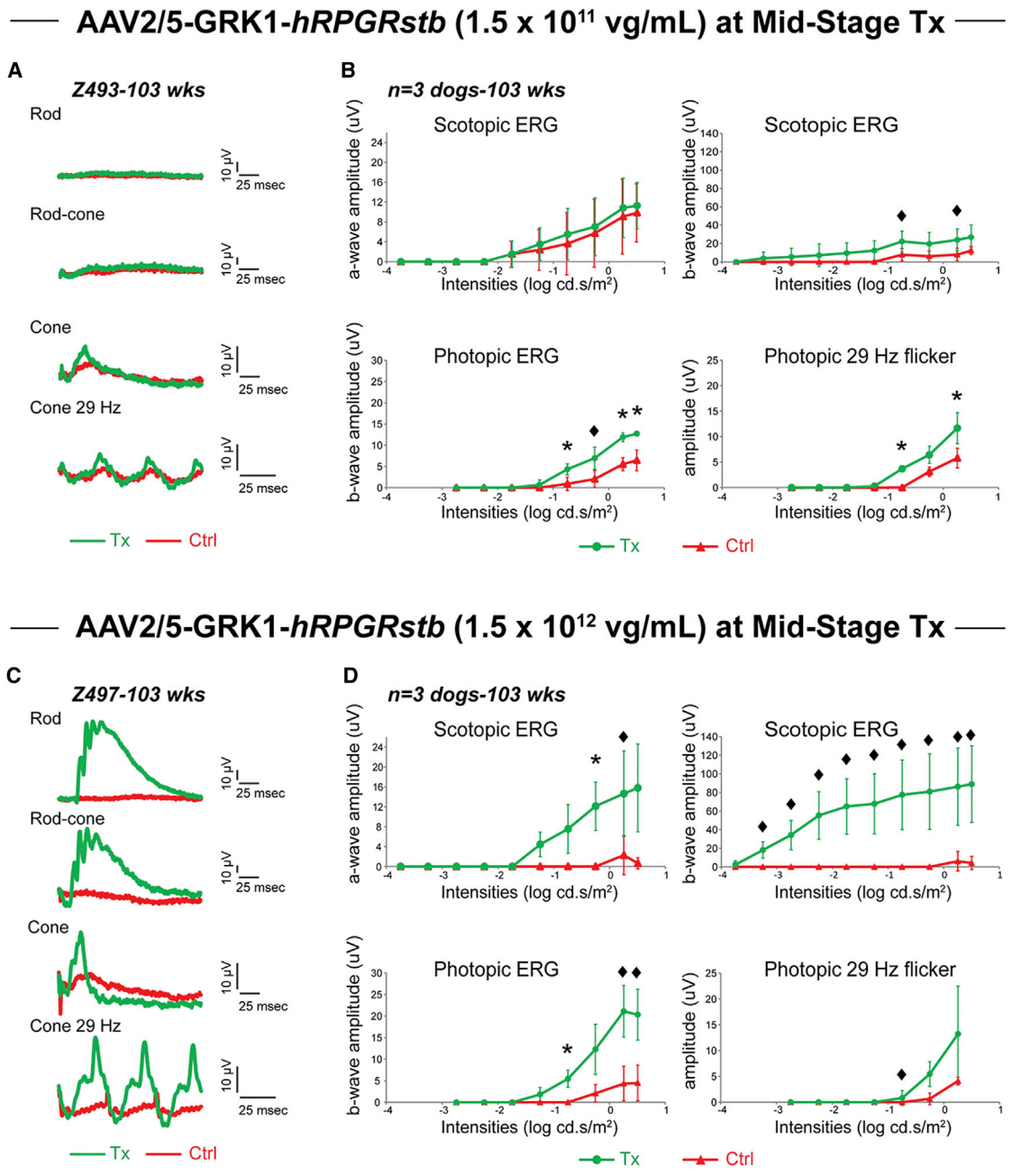

Figure 4. Long-Term Preservation of Retinal Function after Gene Therapy with AAV2/5-GRK1-*h*RPGRstb in Dogs Treated at Mid-stage Disease

(A) Representative ERG traces of rod (−1.74 log cd.s.m^{-2}), mixed rod-cone (1.01 log cd.s.m^{-2}) recorded dark adapted, and cone (1.01 log cd.s.m^{-2}) responses to single stimuli or 29-Hz cone flicker (0.76 log cd.s.m^{-2}) recorded light adapted at 103 weeks of age in an *RPGR* mutant dog treated at 12 weeks of age with 150 µL of a low viral titer (1.51×10^{11} vg/mL). (B) Mean (± SD) of all rod and cone ERG results recorded at 103 weeks of age from three *RPGR* mutant dogs treated at mid-stage disease with 150 µL of a low viral titer (1.51×10^{11} vg/mL). (C) Representative ERG traces in an *RPGR* mutant dog treated at 12 weeks of age with 150 µL of a high viral titer (1.51×10^{12} vg/mL). (D) Mean (± SD) of all rod and cone ERG results recorded at 103 weeks of age from three *RPGR* mutant dogs treated at mid-stage disease with 150 µL of a high viral titer (1.51×10^{12} vg/mL). Tx, treated; Ctrl, contralateral BSS injected; ◆$p \leq 0.07$; *$p < 0.05$; **$p < 0.001$ from paired t test between treated and contralateral eyes.

amplitudes of scotopic and photopic ERG parameters from treated eyes were higher than those of control eyes, with a difference in cone-mediated ERG amplitudes that reached statistical significance ($p < 0.05$, paired t test) under some light intensities above −1 log cd.s/m^2. All three retinas injected with the 1.5×10^{12} vg/mL titer showed improvement of both rod and cone function in comparison

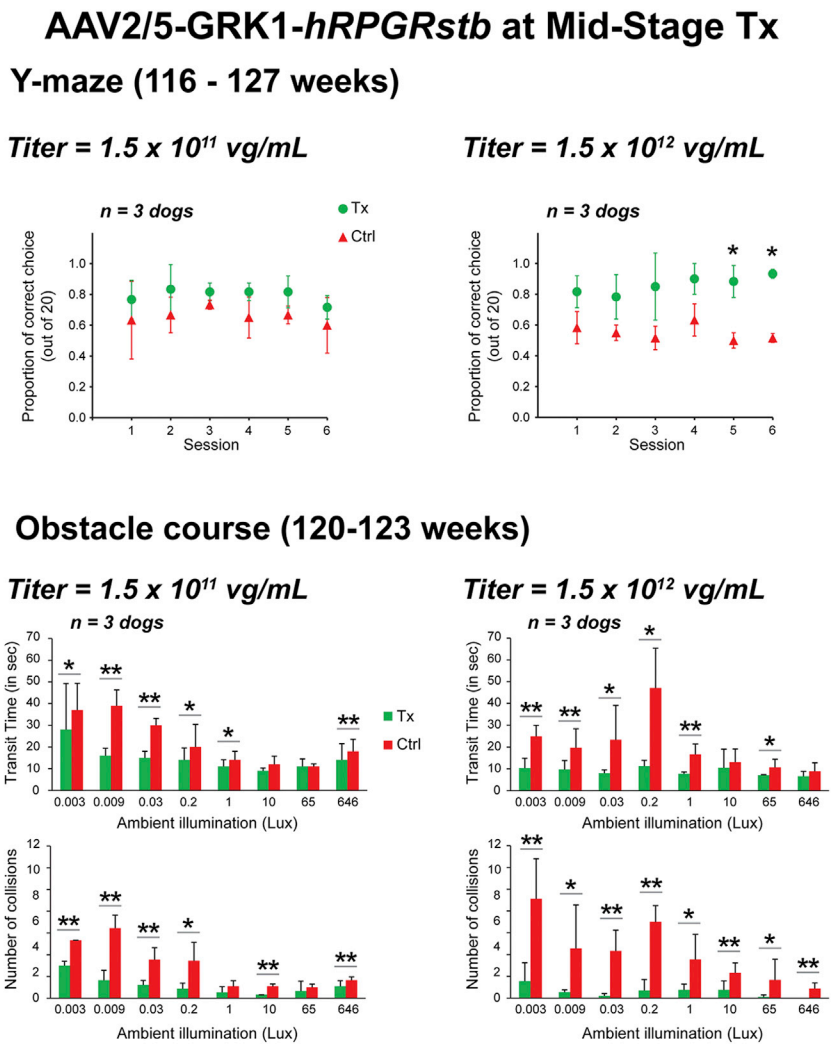

Figure 5. Long-Term Durability of Visual Behavior Rescue after Gene Therapy with AAV2/5-GRK1-*hRPGRstb* in *RPGR* Mutant Dogs Treated at Mid-stage Disease

(A) Visually guided behavior in a forced two-choice Y maze of *RPGR* mutant dogs treated at 12 weeks of age and tested during six sessions between 116 and 127 weeks of age. The performance (mean ± SD) of treated versus contralateral eyes (20 trials per eye per session) are shown from dogs (n = 3 eyes per treatment group) injected with 150 μL of two different titers of viral vector (left and right panels). (B) Visually guided navigational skills in an obstacle-avoidance course under eight different ambient illuminations at 120–123 weeks of age. Top panels show the transit time (mean + SD) and bottom panels show the number of collisions (mean + SD) from the treated versus contralateral eyes of the same dogs shown in (A). Tx, treated; Ctrl, contralateral BSS injected; *p < 0.05; **p < 0.001 from comparisons between treated and contralateral eyes using the paired t test.

to BSS-injected contralateral retinas (Figures 4C and 4D). The differences in amplitudes between treated and BSS-injected eyes were, however, smaller for Z495, which had a more limited region of its retina treated with the viral vector. When taken together, the results from these three dogs, the differences in rod- and cone-mediated ERG amplitudes were statistically significant ($p < 0.05$, paired t test) or marginally significant ($p \leq 0.07$) (Figure 4D) under most light intensities. Comparison of the treatment effects conferred by both viral titers showed improved ERG rescue with all intensities and conditions in eyes treated with the higher (1.5×10^{12} vg/mL) titer (Tables S3–S6). Statistically significant differences ($p < 0.05$, two-sample t test) in scotopic ERG amplitudes were found between the two treatment titers under light intensities ≥ -0.25 log cd.s/m^2 (ERG a wave), and ≥ -2.24 log cd.s/m^2 (ERG b wave). Taken together, these results suggest that while a positive rescue effect on rod and cone function was observed with both titers, a more potent effect on rod-mediated ERG function was obtained with the higher (1.5×10^{12} vg/mL) titer.

Next, rod-mediated visual behavior was evaluated between 116 and 127 weeks of age in the same mid-stage treated *RPGR* mutant eyes. This behavioral test was based on the dogs' ability to detect a dim blue flashing light that was randomly turned on at one of the exits of a forced two-choice Y maze under scotopic conditions. Two out of three retinas that were injected with the 1.5×10^{11} vg/mL titer had a higher success rate than the control retinas during all six testing sessions (Figure S4, left panels), resulting in a higher mean success rate in favor of the treated eyes (Figure 5A, left panel). Three out of three retinas that were injected with the 1.5×10^{12} vg/mL titer had a higher success rate than the control retinas during all six testing sessions (Figure S4, right panels). This resulted in a higher mean success rate in favor of the treated eyes (Figure 5A, right panel), which was found to be statistically significant ($p < 0.05$, paired t test) in two out of six testing sessions. Of the three retinas treated with the 1.5×10^{12} vg/mL titer, Z495-OD had the smallest treated area, which resulted in lower ERG amplitudes when compared to the two other retinas, yet it had the best rescue in ONL thickness of the central retina, which likely explains the better performance in the Y maze. The treatment effect (defined as the difference in success rate between treated and control eyes) for all six sessions combined was significantly higher in the 1.5×10^{12} than in the 1.5×10^{11} vg/mL titer group (0.31 versus 0.14; $p = 0.0005$; two-sample t test).

An obstacle-avoidance course[17,20] was also used to evaluate the visual navigational skills of these animals between 120 and 123 weeks of age. Each eye was tested individually under eight increasing ambient illuminations that ranged from scotopic to photopic conditions. Treatment of retinas with the 1.5×10^{11} vg/mL titer led to a mean transit

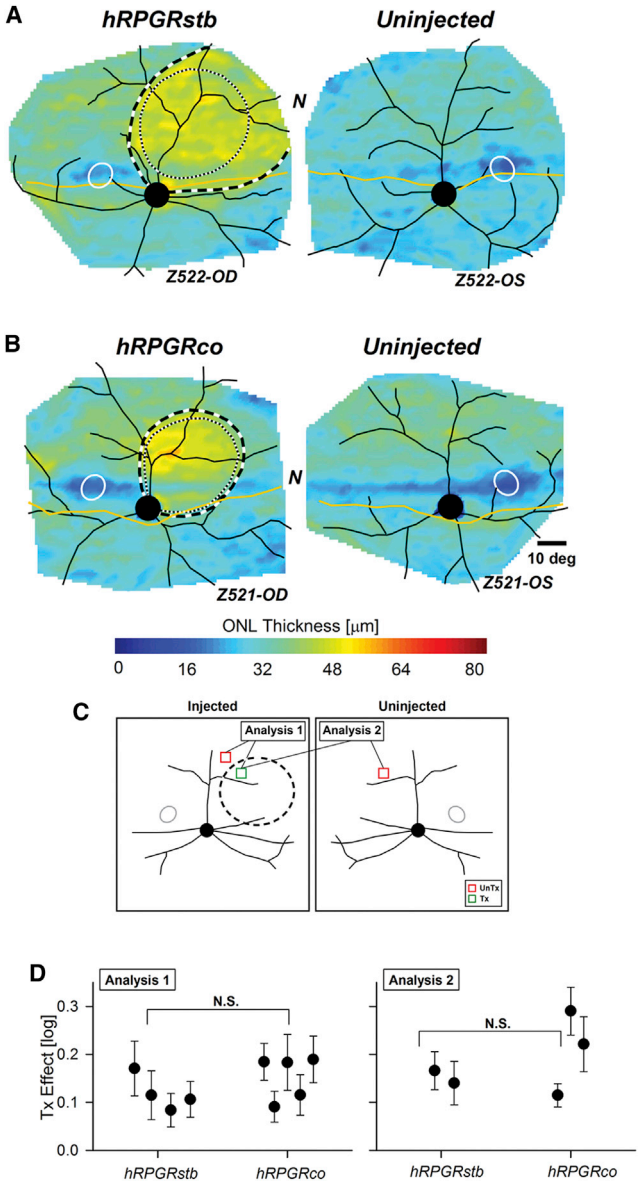

Figure 6. Comparative Efficacy of Two RPGR Gene Constructs at Preserving ONL Thickness

(A and B) ONL thickness topography in individual eyes injected at 5 to 6 weeks of age with 70 μL of a AAV2/5-GRK1-viral vector (titer: 7.2×10^{11} vg/mL) carrying either *hRPGRstb* (A) or *hRPGRco* (B) gene constructs compared with uninjected control eyes. Treatment boundaries are based on fundus photographs of the bleb taken at the time of the injection (dotted lines), and, if visible, demarcations apparent on infrared imaging at the time of scanning (dashed lines). All eyes shown with optic nerve and major blood vessels (black), tapetum boundary (yellow), and fovea-like region (white ellipse) overlaid for ease of comparison. N, nasal retina. Z522-OD and similar labels designate the individual animal and eye. (C) Schematic describing the two methods of analysis performed to compare the efficacy of the two gene constructs. Analysis 1 uses an intra-retinal control and compares the paired loci across the treatment boundary in each eye. Analysis 2 uses the contralateral control eye and compares the loci within the treatment boundary (dashed outline) with loci at corresponding locations in uninjected contralateral eye. UnTx (red squares), untreated; Tx (green squares), treated with vector. (D) Treatment effect (difference in ONL thickness between treated and untreated retina in $\log_{10}$ units), quantified at ~12 weeks after treatment using intra retinal (left) and contralateral (right) control to evaluate efficacy of *hRPGRstb* and *hRPGRco* gene constructs. Symbol with error bars represents mean (± SD) treatment effect for an individual eye in each group of *RPGR* mutant dogs. N.S., not significant, t test.

time and number of collisions that was significantly and statistically reduced in comparison to control eyes under six out of eight illumination conditions (Figure 5B, left panels). Treatment of retinas with the 1.5×10^{12} vg/mL titer led to a mean transit time that was significantly and statistically reduced in comparison to control eyes under six out of eight illumination conditions (Figure 5B, right top panel), whereas the number of collisions was found to be significantly reduced under all eight scotopic to photopic ambient illuminations (Figure 5B, right lower panel).

Taken together, these ERG and visual behavioral studies suggest that RPGR gene augmentation therapy provided rescue of both rod- and cone-mediated vision, and that better results were achieved with the higher titer (1.5×10^{12} vg/mL).

Comparison of Two *hRPGR* Transgenes

The *hRPGRstb* transgene used above and in previous work[12,15–17] was compared to a newly designed *hRPGRco* gene construct (Figure S5) in a cohort of seven *RPGR* mutant dogs (14 eyes): five eyes received AAV2/5-GRK1-*hRPGRco*, four eyes received AAV2/5-GRK1-*hRPGRstb*, and the remaining five eyes were uninjected controls (Figures 1D and 1E; Table S2). Injections were performed at 5 to 6 weeks of age (early-stage disease) with an intermediate titer of 7.2×10^{11} vg/mL, and retinal cross-sectional imaging was performed at 17 to 18 weeks of age. All injections, imaging, and analyses were performed masked to the identity of the vector used in each eye.

ONL thickness topographies from both eyes of two representative dogs qualitatively show the rescue effect resulting from both constructs over the short time interval (Figures 6A and 6B). To compare the two gene constructs quantitatively, two separate analysis methods were used (Figure 6C). Analysis method 1 compared ONL thickness within the treated region to a neighboring intra-retinal untreated control region; this method could be applied to all nine injected eyes. Paired loci were chosen across the treatment boundary and the magnitude of the treatment effect was calculated for each eye. Analysis method 2 compared the ONL thickness within the treated region to an equivalent region in the uninjected contralateral eye; this method was applicable to the subset of five injected eyes with available contralateral uninjected eyes. The treatment effect with *hRPGRstb* was 0.12 and 0.15 log of preservation with analysis methods 1 and 2, respectively. The treatment effect with *hRPGRco* was 0.15 and 0.21 log with analysis methods 1 and 2, respectively. There were no significant differences that were detectable between the two gene constructs with either analysis method (Figure 6D).

The morphologic rescue with in-life imaging conferred by the two *hRPGR* gene products was further evaluated by histology and

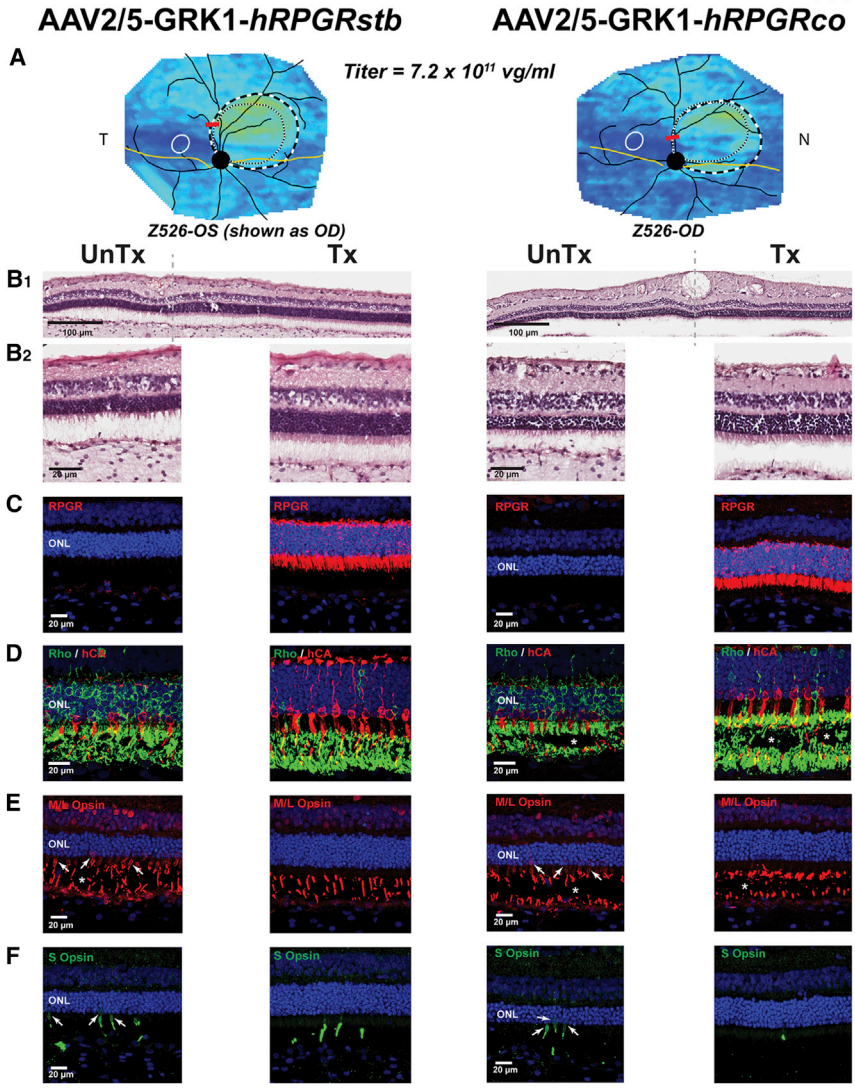

Figure 7. Histological and Immunohistochemical Comparison of Two RPGR Gene Constructs

(A) Pseudocolor maps of ONL thickness at ~17 weeks of age of the eyes of an RPGR mutant dog injected at 5.7 weeks of age with 70 µL of AAV vectors (titer: 7.2×10^{11} vg/mL) carrying either *hRPGRco* or *hRPGRstb* gene constructs. Dotted lines correspond to the border of the bleb based on fundus photographs taken at the time of the injection, and dashed lines correspond to demarcations apparent on infrared imaging at the time of imaging. Eyes are shown as equivalent right eyes with optic nerve and major blood vessels (black), tapetum boundary (yellow), and fovea-like region (white ellipse) overlaid for ease of comparison. N, nasal retina; T, temporal retina. (B–F) Retinal morphology and immunohistochemistry at 23 weeks of age of retinas shown in (A). (B1) H&E-stained section across the treatment boundary shown as a red bar in (A). (B2) H&E stain, higher magnifications view within the untreated (UnTx) and treated (Tx) areas. (C) IHC labeling of the two human RPGR transgene products. (D) Cone arrestin (hCA, red) and rod opsin (Rho, green) double IHC. (E) M/L-opsin IHC labeling. (F) S-opsin IHC labeling. Hoechst 33342 nuclear stain (blue) was used in (C–F). Asterisks, artifactual disruption during sectioning; white arrows point to opsin mislocalization in cones.

immunohistochemistry (IHC) at ~12 and 18 weeks post-injection in treated and untreated areas of the same retina (Figure 7). Preserved ONL thickness in the treated versus non-treated area (Figures 7A and 7B) was seen in eight out of eight eyes that could be evaluated. This included three out of three eyes injected with AAV5-GRK1-*hRPGRstb* and five out of five eyes injected with AAV2/5-GRK1-*hRPGRco*. In one eye (Z517-OS) injected with AAV2/5-GRK1-*hRPGRstb*, oblique sectioning of the retina precluded accurate assessment of the ONL thickness. The *hRPGR* transgene expression was specifically assessed with an antibody that recognizes human RPGR (but not canine RPGR). Labeling of hRPGR was seen in rods of the treated area in nine out of nine eyes (Figure 7C) and was found throughout the cell, with the exception of the outer segment, as previously reported.[15,17] This wide distribution of the RPGR transgene product throughout the cell was found to be fixation-induced, as described by others.[21] Indeed, in the absence of any fixation, RPGR IHC staining in WT retina injected with AAV2/5-GRK1-*hRPGRstb* (Figure 1C) showed the typical punctuate labeling consistent with localized expression at the connecting cilium while 10 min of fixation in 4% paraformaldehyde was sufficient to cause an unexpected widespread distribution of RPGR labeling throughout the rest of the cell (Figure S6A). A similar finding was seen in a retina treated with the AAV2/5-IRBP-*hRPGRstb* (Figure 1F) construct (Figure S6B). Single Z plane confocal microscopy imaging failed to show any RPGR transgene expression in cones of the areas injected with either of the two vectors (data not shown). Rescued rod and cone morphology (Figure 7D), in particular of the inner and outer segments, was seen in the eyes where this assessment was possible: three treated with AAV2/5-GRK1-*hRPGRstb* and three treated with AAV2/5-GRK1-*hRPGRco*. In the remaining eyes, photoreceptor morphology could not be assessed due to misalignment or disruption of the inner and outer segments during cryo-sectioning. Rod and M/L cone opsin mislocalization, a feature of photoreceptor disease,[19] was almost or completely absent in the treated areas of all four eyes injected with AAV2/5-GRK1-*hRPGRstb* and in all five eyes injected with AAV2/5-GRK1-*hRPGRco* (Figures 7D and 7E). Similarly, S-cone opsin mislocalization appeared to be corrected by both vectors (Figure 7F).

DISCUSSION

RPGR-XLRP is one of the most common forms of inherited RD without available treatment to date.[22] However, many of the key steps

for clinical translation of *RPGR*-XLRP gene therapy have already been reached and include (1) description of two naturally occurring forms of retinal degeneration in dogs that closely model the human disease both genetically and phenotypically,[11,15,19,23,24] (2) development of a recombinant AAV construct that efficiently targets transgene expression to photoreceptors of the canine retina,[15,25] and (3) proof-of-concept corrective gene therapy studies in dogs demonstrating that *RPGR* gene augmentation arrests retinal degeneration, even when initiated well after significant photoreceptor loss has occurred.[15–17] Initiation of an investigational new drug (IND) application requires optimization of the vector for human application and determination of its preclinical safety. In the current work, we took important steps toward vector optimization.

Promoter Selection for Transgene Expression in Primate Rods and Cones

The RPGR$^{\text{exon 1-ORF15}}$ isoform is expressed in both rods and cones,[26] and mutations in this gene cause a predominantly XLRP phenotype that affects both classes of photoreceptors.[5,7,10] In the dog models of *RPGR*-XLRP, both rods and cones undergo structural and functional alterations[11,15,19,23,24] that can be prevented or rescued with gene augmentation therapy.[15,17] Thus, these findings support development of an optimized viral vector construct for humans that is capable of efficiently driving gene expression in primate rods and cones. In addition to choosing an AAV capsid able to infect photoreceptors, selecting the appropriate promoter is critical for controlling cell specificity and levels of transgene expression. On the basis of the very efficient rescue achieved in proof-of-concept studies in dogs with an AAV2/5-IRBP-*hRPGRstb* construct and reports on the expression of IRBP both at the mRNA and protein level in human cones,[27,28] we initially considered using the IRBP promoter to drive the therapeutic transgene expression in primate photoreceptors. Unexpectedly, we found that in the macaque retina, the 235-nt portion of the proximal human IRBP promoter drove expression of the *GFP* reporter gene in rods but not cones. Although this portion of the human IRBP promoter includes the regulatory elements for CRX[29] and OTX2,[30,31] two transcription factors critical for retinal development and photoreceptor differentiation,[32] the absence of the IRBP enhancer element[30] located 5′ upstream of the 235-nt sequence used in our constructs may have led to low and undetectable levels of transgene expression in primate cones. This current study confirmed the findings of a previous report[18] by showing that the human GRK1 promoter does drive transgene expression in both rods and cones of NHPs. It must be noted that although both viral titers (1.5×10^{11} and 1.5×10^{12} vg/mL) led to transgene expression in rods, this was achieved in cones only with the higher titer. Should higher levels of the therapeutic transgene be required in cones, this potential limitation may be circumvented by using AAV capsid serotypes reported to have improved tropism to NHP cones than that of AAV2/5.[33,34] However, on the basis of our prior experience with AAV2/5's ability to infect canine rods and cones, this serotype was selected to test whether *hRPGR* transgenes under the control of the GRK1 promoter can result in photoreceptor rescue in the *RPGR* mutant dog.

AAV2/5-GRK1-*hRPGRstb*: Efficacy in the Canine Model

Conflicting results about human GRK1 promoter efficiency at driving transgene expression in canine cones have been published. An AAV2/5-GRK1-e*GFP* vector construct that included the same 292-nt proximal GRK1 promoter region (positions −112 to +180 based on the Khani et al.[14] sequence) as employed in this current study targeted both rods and cones of the WT canine retina, but only when subretinally injected at a high viral titer (1.5×10^{13} vg/mL).[25] At 1.5×10^{12} vg/mL and lower, GFP expression was found exclusively in rods.[25] Using an AAV2/5-GRK1-*eGFP* vector that carried a shorter (199 nt) region of the proximal GRK1 promoter (positions −112 to +87 based on the Khani et al.[14] sequence), strong expression of GFP was shown by another group in both rods and cones of WT dogs with a significantly lower (1×10^{11} vg/mL) titer.[35] This difference may be explained by inter-laboratory differences in viral titration methods. Alternatively, the longer 292-nt sequence of the proximal region of the GRK1 promoter may contain a silencer region not included in the shorter (199 nt) version. A side-by-side comparison of these two promoter versions, driving the expression of an identical reporter gene, packaged in the same AAV pseudotype by the same laboratory, and subretinally delivered to dogs with identically low pre-injection neutralizing antibody titers may help address this discrepancy.

In spite of the apparent lower efficiency of the 292-nt-long GRK1 promoter in comparison to the IRBP promoter (Figure S5), both cone and rod rescue was achieved in a single *RPGR* mutant (XLPRA2) dog injected at 5 weeks of age with AAV2/5-GRK1-*RPGRstb* at 1.5×10^{11} vg/mL.[15] In the current study, we have confirmed that this same vector construct promotes long-lasting (>2 years) ONL preservation and sustains ERG function and visual behavior, but that efficiency is improved with a 10-fold higher titer (1.5×10^{12} vg/mL). Although the lower titer (1.5×10^{11} vg/mL) did not result in rod-mediated ERG responses, improved navigational skills under scotopic illumination was detectable in the obstacle course. These results are not surprising because limited areas of surviving rods can confer vision retention while their function may remain undetectable by full-field ERG. More surprising is the retention of cone ERG function in light of the absence of transgene expression in cones. Retinas injected with an intermediate titer (7.2×10^{11} vg/mL) also showed ONL thickness rescue in the treated area and correction of both rod and cone opsin mislocalization, but no expression of the *hRPGR* transgene was detected in cones by IHC. Although it cannot be excluded that cone rescue is indirect and secondary to rod preservation,[36] these results also suggest that the GRK1 promoter used in this study may drive the expression of undetectable yet sufficient levels of hRPGR in canine cones. In addition, the demands for RPGR expression may be lower for cones than for rods to remain functional. Proof-of-concept gene therapy studies utilizing this promoter in dogs may therefore still provide a positive outcome if the augmentation strategy requires delivery of limited amounts of the transgene product in cones. Correcting the cone phenotype in canine models of retinal ciliopathies by expressing sufficient levels of proteins, such as RPGR, RPGRIP, or NPHP5/IQCB1, at the cone-connecting cilium appears

indeed achievable with the GRK1 promoter.[15,35,37] Positive rescue of cones using a promoter that is weaker in dogs than in NHPs may therefore provide a rationale for considering testing within the context of a future clinical trial an AAV2/5-GRK1-hRPGR vector at viral titers lower than 1.5×10^{12} vg/mL.

Two *hRPGR* Transgenes Efficiently Rescue Photoreceptors in the *RPGR* Mutant Dog

The *RPGR* cDNA contains a long purine-rich repetitive sequence in the ORF15 exon that is unstable during recombinant DNA manipulation. This complicates efforts to develop AAV-based vectors for gene therapy. A stabilized, yet shortened version of *hRPGR* cDNA (*hRPGRstb*)[12] was shown to effectively rescue photoreceptors in two canine models of *RPGR*-XLRP.[15,17] Efforts to obtain the full-length human *RPGR*-ORF15 cDNA and maintain its integrity during cloning and plasmid propagation in a conventional bacteria strain have generally been unsuccessful. Recently, it was reported that after testing various *Escherichia coli* strains, the vector plasmids containing either human or mouse *RPGR* cDNAs maintained their integrity in XL10 Gold cells, although minor deletions were readily detected in some of the AAV vector preparations.[21] We reasoned that the stability of *RPGR*-ORF15 cDNA could be significantly improved by rational design of the cDNA sequence through codon modification without changing the amino acid sequence, and successfully achieved a codon-optimized cDNA (*hRPGRco*) that is stable through multiple passages in plasmids, in recombinant herpes simplex viruses, and during production of AAV vectors.[38] Side-by-side comparison of the *hRPGRstb* and *hRPGRco* transgenes delivered to *RPGR* mutant dogs at early-disease stage showed a similar level of ONL rescue and structural preservation of rods and cones. Such changes will facilitate the manufacture of therapeutic vectors for clinical trials.

In summary, we have optimized an AAV vector construct to enable efficient transduction of both rods and cones in the primate retina and have validated in a large animal model of *RPGR*-XLRP the long-term efficacy of this optimized treatment when delivered after the onset of substantial photoreceptor loss. Taken together, our results suggest that an AAV vector carrying a stabilized full-length human *RPGR* cDNA under the control of a human GRK1 promoter can be considered for translation into a clinical trial.

MATERIALS AND METHODS

AAV Vector Preparation

The AAV2/5-IRBP-e*GFP* and AAV2/5-GRK1-e*GFP* vectors (Figures 1A and 1B) used in NHP experiments contained a humanized enhanced version of the GFP cDNA (*eGFP*) downstream of either the 235-nt segment of the proximal human IRBP promoter[13] or the 292-nt portion of the human GRK1 promoter (positions −112 to +180 based on the Khani et al.[14] sequence) used in previous *RPGR* gene augmentation experiments in dogs[15–17] with a stabilized cDNA sequence of human $RPGR^{\text{exon 1-ORF15}}$ (*hRPGRstb*).[12] The composition and placement of all other elements (e.g., SV40 splice donor/acceptor site and polyadenylation signals) was identical to that of the AAV2/5-IRBP-*hRPGRstb* and AAV2/5-GRK1-*hRPGRstb* constructs (Figures 1C and 1F). Four different vector constructs (Figures 1C–1F) were used in dogs and included AAV2/5-GRK1-*hRPGRstb* (Figure 1C) and AAV2/5-IRBP-*hRPGRstb* (Figure 1F), which have been previously described,[12,15,17] a new AAV2/5-GRK1-*hRPGRstb* construct with no bovine growth hormone poly A (bGH pA) signal (Figure 1D), and a slightly modified 295-nt-long segment of the proximal GRK1 promoter (positions 1793–2087, GenBank AY327580) and an AAV2/5-GRK1-*hRPGRco* construct (Figure 1E) that contained a similar 295-nt-long GRK1 promoter driving the expression of a full-length codon-optimized human $RPGR^{\text{exon 1-ORF15}}$ cDNA (*hRPGRco*). The *hRPGRco* cDNA sequence (Figure S5) was designed based on GenBank reference mRNA sequence NM_001034853, which encodes *hRPGR* isoform C. The 3,459-bp coding sequence was codon optimized based on human codon usage and further modified to reduce tandem repeats and adjust G/C content, where possible. It was then synthesized and cloned into various plasmid vectors, including an AAV vector plasmid (used for AAV production by transfection). AAV2/5 vectors were packaged by plasmid transfection of HEK293 cells and virus purified by iodixanol density gradient, followed by fast protein liquid chromatography (FPLC) chromatography using published methods.[39] Stability of the *hRPGRco* cDNA sequence (GenBank KY293401) was verified by DNA sequencing at multiple steps, which confirmed there were no DNA sequence changes after subcloning into an AAV production plasmid, large-scale production of the AAV production plasmid, and from the AAV vector produced using the AAV production plasmid. The ability of the *hRPGRco* cDNA to direct synthesis of a full-length hRPGR protein was also verified by western blot analysis of HEK293 cells transiently transfected with plasmid pTR-CBA-hRPGRco (containing a chicken beta-actin promoter) or infected with the AAV vectors AAV-CBA-hRPGRco or AAV-GRK1-hRPGRco (containing the GRK1 promoter) (Figure S7). Stability of the *hRPGRstb* cDNA sequence was also verified by DNA sequencing of the AAV production vector and the AAV vector produced using the AAV production vector, which demonstrated no changes. Based on these data, the codon-optimized vector is at least as effective as the stabilized, shorter version of the vector.

The virus was concentrated and resuspended in BSS (Alcon) supplemented with 0.014% Tween 20. Titering was performed by quantitative real-time PCR relative to a standard. Vector preparations were assessed by silver-stained SDS-PAGE to visualize capsid proteins VP1, VP2, and VP3 and confirm the absence of contaminating protein. Additionally, all vector preparations were tested and confirmed to be free of endotoxin (<5 EU/mL).

Animals

Two closely related species of macaques (*Macaca mulatta* and *Macaca fascicularis*) were used in this study and housed at the University of Alabama at Birmingham (Table S1). The use of two macaque species was based on availability of the animals. With the exception of three WT beagles purchased from a commercial vendor, the dogs were bred and maintained at the University of Pennsylvania

Retinal Disease Studies Facility (RDSF) (Table S2). Studies in NHPs and dogs were carried out in strict accordance with the recommendations in the Guide for the Care and Use of Laboratory Animals of the National Institutes of Health in compliance with the USDA's Animal Welfare Act, Animal Welfare Regulations, and ARVO Statement for the Use of Animals in Ophthalmic and Vision Research. The protocols were approved by the Institutional Animal Care and Use Committee of the University of Pennsylvania and University of Alabama at Birmingham.

All electroretinographic and noninvasive imaging procedures, as well as subretinal injections, were performed under general anesthesia, as previously described,[15,17,18,40] and all efforts were made to improve animal welfare and minimize discomfort. Included in this study were eight eyes from four NHPs (Table S1), 24 eyes from 15 WT dogs, and 30 eyes from 15 *RPGR* mutant dogs (Table S2).

Neutralizing Antibody Assays

Serum samples from NHPs were screened prior to purchase for the presence of anti-AAV5 neutralizing antibodies using methods previously described.[18] Briefly, self-complimentary AAV5-smCBA-mCherry vector (10^4 genomic copies per cell) was diluted in serum-free DMEM/F-12 1:1 modified medium and incubated with 2-fold serial dilutions (from 1:10 to 1:1,280) of heat-inactivated NHP serum samples or naive mouse serum in DMEM/F-12 1:1 modified medium for 1 hr at 37°C. The serum-vector mixture was then used to infect ARPE 19 cells. Three days post-infection, cells were dissociated and 10,000 cells per sample were counted and analyzed using a BD LSR II flow cytometer equipped with BD FACSDIVA 6.2 software (BD Biosciences). Transduction efficiency was calculated by multiplying the percentage of cells positive for mCherry by the mean fluorescence intensity.[41,42] The neutralizing antibody (NAb) titer was reported as the highest serum dilution that inhibited self-complementary AAV5-smCBA-mCherry transduction (mCherry expression) by $\geq$50% compared with mouse naive serum control (cat # S3509, Sigma-Aldrich).

Subretinal Injections

All NHP surgical procedures were carried out under sterile conditions in a dedicated veterinary ophthalmic surgical suite. The subjects were sedated using 100 mg/mL ketamine (10 mg/kg intramuscular [IM]) and given subcutaneous 0.54 mg/mL atropine (0.05 mg/kg). An intravenous (IV) catheter was placed and a saline drip was started, then the animal was intubated. Once deeply sedated, the eyes were dilated using 2.5% phenylephrine, 1% tropicamide, and 1% cyclopentolate. The animal was placed on a ventilator, and general anesthesia was carried out using isoflurane (1.5% maintenance) while vital signs were continuously monitored. The eyes were prepared with Betadine scrub and draped in a standard sterile fashion. An Accurus 800CS surgical system with Xenon light source, Total Plus 23 gauge Vitrectomy Pak (Alcon), and Zeiss VISU 200 ophthalmic surgical microscope equipped with digital video (Endure Medical) were used for the surgery. The posterior segment retina was visualized using an irrigating Machemer magnifying vitrectomy contact lens (Ocular Instruments). A standard 23-gauge three-port pars plana vitrectomy was performed with an inferior infusion cannula maintaining a continuous pressure of 30 mm/Hg with BSS Plus (Alcon). Subsequently, the sclerotomy was enlarged with a 20-gauge MVR blade for the injection cannula. A 39-gauge injection cannula within a 20-gauge shaft (Synergetics) was used to deliver 50–100 μL of vector into the subretinal space at both a macular and a superior temporal site.

In dogs, subretinal injections of BSS or vector were performed under direct visualization through an operating microscope and a contact vitrectomy lens using a subretinal cannula as previously reported.[25,43] Volumes injected (70–150 μL) were adjusted to the dogs' age/globe size aiming to produce a bleb that covered ~1/5 of the retinal surface. The location of the subretinal bleb was recorded by fundus photography (Retcam shuttle, Clarity Medical Systems) immediately after each injection. Injections in mutant dogs were performed either at ~5 to 6 weeks of age (early-stage disease, no ONL thinning) or at 12 weeks of age, corresponding to mid-stage disease (~40% loss of photoreceptors).

In Vivo Confocal Scanning Laser Ophthalmoscopy and Optical Coherence Tomography Imaging and Analyses

En face and retinal cross-sectional imaging was performed with the dogs under general anesthesia. Overlapping en face images of reflectivity with near-infrared illumination (820 nm) were obtained (Spectralis HRA+OCT) with 30° and 55° diameter lenses to delineate fundus features, such as optic nerve, retinal blood vessels, boundaries of injection blebs, retinotomy sites, and other local changes. Custom programs (MATLAB 7.5; The MathWorks) were used to digitally stitch individual photos into a retina-wide panorama. In a subset of eyes, short-wavelength autofluorescence and reflectance imaging were used to outline the boundary of the tapetum and pigmented RPE.

Spectral-domain optical coherence tomography (SD-OCT) was performed with linear and raster scans (Spectralis HRA+OCT). Overlapping (30° × 20°) raster scans were recorded covering large regions of the retina. Post-acquisition processing of OCT data was performed with custom programs (MATLAB 7.5). For retina-wide topographic analysis, integrated backscatter intensity of each raster scan was used to locate its precise location and orientation relative to retinal features visible on the retina-wide mosaic formed by NIR reflectance images. Individual longitudinal reflectivity profiles (LRPs) forming all registered raster scans were allotted to regularly spaced bins (1° × 1°) in a rectangular coordinate system centered at the optic nerve; LRPs in each bin were aligned and averaged. Intraretinal peaks and boundaries corresponding to the ONL were segmented using both intensity and slope information of backscatter signal along each LRP. For all topographic results, locations of blood vessels, optic nerve head, bleb, tapetum boundaries, and fovea-like area[44] were overlaid for reference.

First, all normal ONL maps from WT dogs were registered by the centers of the optic nerve head and rotated to bring the fovea-like areas in

congruence and a map of mean WT ONL thickness was derived. The fovea-like area of *RPGR* mutant dogs was determined by superimposing a WT template onto mutant eyes by alignment of the optic nerve head, major superior blood vessels, and the boundary of the tapetum. Next, *RPGR* mutant ONL maps were registered to the WT map by the center of the optic nerve and estimated fovea-like area, and an ONL fraction was derived by dividing each ONL thickness sample by the corresponding mean WT value. This derived ONL fraction map was sampled across the treatment boundary at supero-nasal locations chosen individually for each eye. To measure a short-term durability of gene therapy, a treatment effect was quantified at paired locations as a difference between ONL fraction within and outside the treatment boundary. Comparison of ONL thickness in retinas injected with AAV2/5-GRK1-*hRPGRstb* versus AAV2/5-GRK1-*hRPGRco* was done with the investigators masked.

ERG Recording and Analyses

Dogs were pre-medicated with subcutaneous injections of atropine and acepromazine, and their pupils were dilated with atropine (1%), tropicamide (1%), and phenylephrine (10%). After induction with intravenous propofol, dogs were maintained under general inhalation anesthesia (isoflurane), and their pulse rate, oxygen saturation, and temperature were monitored for constancy during the entire procedure. Full-field flash ERG was performed on both eyes using a custom-built Ganzfeld dome fitted with the light-emitting diode (LED) stimuli of a ColorDome stimulator (Diagnosys). After 20 min of dark adaptation, rod and mixed rod-cone mediated responses (averaged four times) to a single 4-ms white flash stimuli of increasing intensities (from −3.74 to 0.51 log cd.s.m^{-2}) were recorded. Following 5 min of white light adaptation (1.53 log cd.m^{-2}), cone-mediated signals (averaged ten times) to a series of single flashes (from −2.74 to 0.51 log cd.s.m^{-2}) and a 29.4-Hz flicker (averaged 20 times; from −2.74 to 0.26 log cd.s.m^{-2}) stimuli were recorded. Waveforms were processed with a digital low-pass (50 Hz) filter to reduce recording noise if necessary. Amplitudes of the a- and b-waves of the scotopic ERG, and the peak-to-peak amplitudes of the photopic single flash and 29.4-Hz flicker were measured. Mean and standard deviation of these ERG parameters were calculated for the treated eyes and BSS-injected contralateral eyes of the low-dose-treated dogs and the high-dose-treated dogs (n = 3 dogs/dose group). Comparison of ERG parameters between treated and contralateral eyes were made using a paired t test. The comparisons of treatment effect (defined as the difference between treated eye minus the contralateral eye of each dog for each ERG measure) between the low dose and the high dose were performed using a two-sample t test. All statistical analyses were performed using SAS v9.4 (SAS Institute), and two-sided $p < 0.05$ was considered statistically significant.

Visual Behavior Testing in a Y Maze

A custom-built Y maze for dogs whose technical specifications have been recently described[17] was used to test the ability of *RPGR* mutant dogs to detect a faint stimulus (50-ms duration) created by a strip of six blue flickering (3 Hz) LEDs (470 nm) that produced at dog's eyes level a corneal irradiance of $\sim 1 \times 10^{-6}$ mW/cm^2 measured with an illuminometer (IL1700, International Light Technologies). Following a period of socialization, during which bright sources of white light (6,500 K; stimulus: 3 Hz, 50-ms duration; corneal irradiance at bifurcation: 6.25 mW/cm^2) delivered by strips of six LEDs (Nemalux) were used to train the dogs at selecting the correct (illuminated) exit, the animals were tested under scotopic conditions with the significantly dimmer blue light stimuli. Each eye was tested separately by placing a black ocular shield (Aestek, Oculo-plastik) on the contralateral eye. Random selection of the eye to be tested first was made before the session. After a dark adaptation period of 20 min, the dog was run in the Y maze 20 times for each eye. Only one strip of LEDs was randomly turned on for any given trial. Both the right and left light stimuli were turned on 10 times. Once the dog had completed its 20 trials for one eye, the contralateral eye was subsequently tested. Testing occurred during six sessions between 116 and 127 weeks of age. An infrared sensitive camera placed inside the Y maze recorded the choice of the dog when it entered the bifurcation. An experienced observer who was masked to the experimental treatment reviewed all the videos and recorded for each eye the number of times (out of 20 trials) that the dog correctly selected the illuminated exit. The proportion of correct exit choices (out of 20 trials) between the treated (AAV2/5-GRK1-*hRPGRstb*) and contralateral (BSS-injected) fellow eye of each of the three *RPGR* mutant dogs (per dose group) was compared by the Fisher exact test at each of the six testing sessions. Comparison of mean success rate between treated eyes and control eyes (n = 3 animals) was performed using a paired t test at each session. For comparison of treated eyes and contralateral eyes when considering all sessions together, the generalized linear models using generalized estimating equations (GEEs) was applied to account for the correlation among repeated measurements from the same animal.[45] Comparison of the treatment effect (defined as the difference in proportion of exit choice between the treated eye and the contralateral eye in the same dog) between the low dose and high dose was performed by using a two-sample t test. All statistical analyses were performed using SAS v9.4 (SAS Institute), and two-sided $p < 0.05$ was considered statistically significant.

Visual Behavior Testing in an Obstacle-Avoidance Course

After a period of socialization and training, visually guided behavior was evaluated with a 3.6-m-long custom-built obstacle-avoidance course[20] that includes five displaceable panels and that was recently used to objectively assess visual navigational skills of *RPGR* mutant dogs treated with an AAV2/5-IRBP-*hRPGRstb* vector.[17] Eyes were tested individually by placing a black ocular shield (Aestek, Oculo-plastik) on the contralateral cornea. Both eyes were tested three times under each of the eight distinct ambient illuminations that ranged from scotopic (0.003, 0.009, and 0.03 lux) to mesopic (0.2 and 1 lux) to photopic (10, 65, 646 lux) conditions. These light intensities were calibrated with a light meter (IL1700, International Light Technologies) at the level of dog's eye. The position of the five panels was randomly changed between each of the three trials per eye per illumination level. The contralateral eye was tested with the same set of panel positions. Random selection of the eye to be tested first was made before the session.

For this assessment, dogs were first adapted for 20 min to the lowest ambient illumination (0.003 lux) before running through the course; subsequently, the illumination was increased to the next level of brightness, and dogs were adapted for 10 min and tested as previously described. A session was considered complete when testing under the eight ambient illuminations was performed (total of 48 trials), which occurred on separate days during the 120–123 weeks of age time period. Two digital cameras (Sony Handycam, DCR-DVD108, Sony) located above the obstacle course recorded the navigation performance of the dogs. The infrared imaging function of the camera enabled recording under the dimmest light conditions. An experienced observer who was masked to the experimental treatment reviewed the videos of each trial to acquire the two following parameters: transit time (in seconds) through the obstacle course and total number of collisions into the walls or moveable obstacle panels. The mean transit time and number of collisions under each ambient illumination were calculated for treated eyes and the contralateral BSS-injected eyes of each dose group. The comparison of transit time and number of collisions between treated eyes and their contralateral eyes in each dose group was performed using generalized linear models, with GEEs to account for the inter-eye correlation and correlation from multiple trials.[45] All statistical analyses were performed using SAS v9.4 (SAS Institute), and two-sided $p < 0.05$ was considered statistically significant.

Tissue Preparation, IHC, and Microscopy

NHPs were euthanized and perfused, and their eyes were enucleated at 8 weeks post-injection with AAV2/5-IRBP-e*GFP* or 10 weeks post-injection with AAV2/5-GRK1-e*GFP* according to previously published methods.[18] The retinas were divided into 5- by 8-mm blocks for ease of cryoprotection/sectioning, and each block was photographed for later orientation. Blocks were positioned for sectioning in the sagittal plane. Tissue embedding and cryoprotection in two parts 30% sucrose and 1 part Histoprep (Fisher Scientific) were performed as described.[18] 10-μm-thick retinal sections were cut on a Leica CM3050 S cryostat (Leica), and detailed notes were kept to keep track of every section and whether that section was mounted or discarded. This, combined with landmarks in block photographs, allowed for orientation within the retina. NHP retinal sections were immunostained and imaged using a previously published protocol,[18] with minor modifications. Tissue was stained with primary antibody generated against human cone arrestin ("Lumif," generously provided by Dr. Cheryl Craft, University of Southern California) diluted 1:30,000 to label cone photoreceptors, followed by incubation in an immunoglobulin G (IgG) secondary antibodies tagged with either 594 or Cy5 fluorophores. Sections were then incubated in autofluorescence eliminator reagent (Cat. #2160; EMD Millipore) and counterstained with DAPI. All NHP sections were imaged using spinning disk confocal microscopy (Nikon Eclipse TE2000 microscope equipped with Perkin Elmer Ultraview Modular Laser System).

RPGR mutant dogs injected with either AAV2/5-GRK1-*hRPGRstb* or AAV2/5-GRK1-*hRPGRco* (titer: 7.2×10^{11} vg/mL) had their treated and untreated eyes collected immediately after euthanasia with an intravenous injection of euthanasia solution (Euthasol; Virbac). The globes were fixed in 4% paraformaldehyde (PFA) for 3 hr, followed by 2% PFA for 24 hr, trimmed, cryoprotected in 15%–30% sucrose/PBS solution, and embedded in optimal cutting temperature media, as previously reported.[15,17,19] 10-μm-thick serial sections that encompassed the nontreated, boundary, and treated/bleb area were cut on a cryostat (Microm HM550; Thermo Fisher Scientific). Blood vessel landmarks identified by H&E staining were used to determine the precise location of the retinal cryosections on the vascular pattern of the en face cSLO images. Sequential sections were immunolabeled with primary antibodies and cell-specific markers: human RPGR (cat# HPA001593; 1:100 dilution; Sigma-Aldrich), rod opsin (cat# MAB5316; 1:200 dilution; EMD Millipore), goat anti-human cone arrestin (W. Beltran, University of Pennsylvania; 1:100), M/L cone opsin (cat#AB5405; 1:100 dilution; EMD Millipore), and S cone opsin (cat #SC-14363; 1:50 dilution; Santa Cruz Biotechnologies). A single WT dog (M704) injected with AAV2/5-GRK1-*hRPGRstb* in one eye and AAV2/5-IRBP-*hRPGRstb* in the other eye had its posterior cups trimmed and embedded without any prior fixation or cryoprotection. Retinal cryosections were either fixed in 4% PFA for 10 min or kept unfixed, and used for RPGR IHC. The antigen-antibody complexes were visualized with fluorochrome-labeled secondary antibodies (Alexa Fluor, 1:200; Molecular Probes), and Hoechst 33342 nuclear stain (Molecular Probes) was used to label cell nuclei. H&E-stained sections were examined by widefield microscopy (Axioplan; Carl Zeiss Meditec), and the images were digitally captured (Spot 4.0 camera; Diagnostic Instruments) and imported into a graphics program (Illustrator; Adobe) for display. Sections labeled for fluorescent IHC were examined by confocal microscopy (Leica TCS SP5; Leica Microsystems), and digital images were taken, processed using the Leica Application suite program, and imported into a graphics program (Illustrator; Adobe). Comparison of the treatment effect in retinas injected with AAV2/5-GRK1-*hRPGRstb* versus AAV2/5-GRK1-*hRPGRco* was done with the investigators masked to the treatment.

SUPPLEMENTAL INFORMATION

Supplemental Information includes seven figures and six tables and can be found with this article online at http://dx.doi.org/10.1016/j.ymthe.2017.05.004.

AUTHOR CONTRIBUTIONS

Conceptualization, W.A.B., S.E.B., G-J.Y., J.D.C., W.W.H., and G.D.A.; Investigation, W.A.B., A.V.C., S.E.B., S.I., V.L.D., L.F.M., J.S., S.L.B., J.J.P., C.D.W., J.J.A., and P.D.G.; Formal Analysis, A.V.C., M.S., M.S.K., and G-S.Y.; Resources, G-J.Y., M.S.S., and J.D.C.; Writing – Original Draft, W.A.B. and A.V.C.; Writing – Review and Editing, W.A.B., A.V.C., S.E.B., G-J.Y., M.S.S., J.D.C., W.W.H., P.D.G, S.G.J., and G.D.A; Supervision, W.A.B.; Funding Acquisition, W.A.B., A.V.C., S.E.B., J.D.C., and G.D.A.

CONFLICTS OF INTEREST

W.A.B., A.V.C., S.L.B., W.W.H., S.G.J., and G.D.A. are listed as inventors on the patent application (PCT/US2013/022628) titled

"AAV-mediated gene therapy for RPGR X-linked retinal degeneration" held by the Trustees of the University of Pennsylvania and licensed to AGTC. W.W.H. and the University of Florida have a financial interest in the use of AAV therapies and own equity in AGTC. G.-J.Y., M.S.S., and J.D.C. are employees of AGTC and own equity in AGTC.

ACKNOWLEDGMENTS

The authors thank Cheryl Craft (University of Southern California) for providing the human cone arrestin ("Lumif") antibody, Joyce Chi for canine anesthesia support, Kendra McDaid and Dana McLaughlin for canine visual behavior testing, Theresa Jordan and the RDSF staff for canine husbandry, Svetlana Savina, Inna Martynyuk, Julie Hill, Debbie Whitten, Deidra Isbell, Myra Rivers, and Tracy Morris for excellent technical assistance, and Lydia Melnyk for research coordination. This work was supported primarily by NEI/NIH (R24EY-022012, R01EY017549, R01EY06855, R01EY013203, R01EY024280, P30EY-001583, and P30EY-003039) and AGTC (Alachua, FL, USA). Additional support provided by the Foundation Fighting Blindness, Macula Vision Research Foundation, Hope for Vision, Van Sloun fund for canine genetic research, and Research to Prevent Blindness.

REFERENCES

1. Bramall, A.N., Wright, A.F., Jacobson, S.G., and McInnes, R.R. (2010). The genomic, biochemical, and cellular responses of the retina in inherited photoreceptor degenerations and prospects for the treatment of these disorders. Annu. Rev. Neurosci. *33*, 441–472.
2. Naldini, L. (2015). Gene therapy returns to centre stage. Nature *526*, 351–360.
3. Thompson, D.A., Ali, R.R., Banin, E., Branham, K.E., Flannery, J.G., Gamm, D.M., Hauswirth, W.W., Heckenlively, J.R., Iannaccone, A., Jayasundera, K.T., et al.; Monaciano Consortium (2015). Advancing therapeutic strategies for inherited retinal degeneration: recommendations from the Monaciano Symposium. Invest. Ophthalmol. Vis. Sci. *56*, 918–931.
4. Wright, A.F. (2015). Long-term effects of retinal gene therapy in childhood blindness. N. Engl. J. Med. *372*, 1954–1955.
5. Vervoort, R., Lennon, A., Bird, A.C., Tulloch, B., Axton, R., Miano, M.G., Meindl, A., Meitinger, T., Ciccodicola, A., and Wright, A.F. (2000). Mutational hot spot within a new RPGR exon in X-linked retinitis pigmentosa. Nat. Genet. *25*, 462–466.
6. Breuer, D.K., Yashar, B.M., Filippova, E., Hiriyanna, S., Lyons, R.H., Mears, A.J., Asaye, B., Acar, C., Vervoort, R., Wright, A.F., et al. (2002). A comprehensive mutation analysis of RP2 and RPGR in a North American cohort of families with X-linked retinitis pigmentosa. Am. J. Hum. Genet. *70*, 1545–1554.
7. Sharon, D., Sandberg, M.A., Rabe, V.W., Stillberger, M., Dryja, T.P., and Berson, E.L. (2003). RP2 and RPGR mutations and clinical correlations in patients with X-linked retinitis pigmentosa. Am. J. Hum. Genet. *73*, 1131–1146.
8. Branham, K., Othman, M., Brumm, M., Karoukis, A.J., Atmaca-Sonmez, P., Yashar, B.M., Schwartz, S.B., Stover, N.B., Trzupek, K., Wheaton, D., et al. (2012). Mutations in RPGR and RP2 account for 15% of males with simplex retinal degenerative disease. Invest. Ophthalmol. Vis. Sci. *53*, 8232–8237.
9. Churchill, J.D., Bowne, S.J., Sullivan, L.S., Lewis, R.A., Wheaton, D.K., Birch, D.G., Branham, K.E., Heckenlively, J.R., and Daiger, S.P. (2013). Mutations in the X-linked retinitis pigmentosa genes RPGR and RP2 found in 8.5% of families with a provisional diagnosis of autosomal dominant retinitis pigmentosa. Invest. Ophthalmol. Vis. Sci. *54*, 1411–1416.
10. Charng, J., Cideciyan, A.V., Jacobson, S.G., Sumaroka, A., Schwartz, S.B., Swider, M., Roman, A.J., Sheplock, R., et al. (2016). Variegated yet non-random rod and cone photoreceptor disease patterns in RPGR-ORF15-associated retinal degeneration. Hum. Mol. Genet. *25*, 5444–5459.
11. Zhang, Q., Acland, G.M., Wu, W.X., Johnson, J.L., Pearce-Kelling, S., Tulloch, B., Vervoort, R., Wright, A.F., and Aguirre, G.D. (2002). Different RPGR exon ORF15 mutations in Canids provide insights into photoreceptor cell degeneration. Hum. Mol. Genet. *11*, 993–1003.
12. Deng, W.T., Dyka, F.M., Dinculescu, A., Li, J., Zhu, P., Chiodo, V.A., Boye, S.L., Conlon, T.J., Erger, K., Cossette, T., et al. (2015). Stability and safety of an AAV vector for treating RPGR-ORF15 X-linked retinitis pigmentosa. Hum. Gene Ther. *26*, 593–602.
13. al-Ubaidi, M.R., Font, R.L., Quiambao, A.B., Keener, M.J., Liou, G.I., Overbeek, P.A., and Baehr, W. (1992). Bilateral retinal and brain tumors in transgenic mice expressing simian virus 40 large T antigen under control of the human interphotoreceptor retinoid-binding protein promoter. J. Cell Biol. *119*, 1681–1687.
14. Khani, S.C., Pawlyk, B.S., Bulgakov, O.V., Kasperek, E., Young, J.E., Adamian, M., Sun, X., Smith, A.J., Ali, R.R., and Li, T. (2007). AAV-mediated expression targeting of rod and cone photoreceptors with a human rhodopsin kinase promoter. Invest. Ophthalmol. Vis. Sci. *48*, 3954–3961.
15. Beltran, W.A., Cideciyan, A.V., Lewin, A.S., Iwabe, S., Khanna, H., Sumaroka, A., Chiodo, V.A., Fajardo, D.S., Román, A.J., Deng, W.T., et al. (2012). Gene therapy rescues X-linked photoreceptor blindness in dogs and paves the way for treating human X-linked retinitis pigmentosa. Proc. Natl. Acad. Sci. USA *109*, 2132–2137.
16. Beltran, W.A., Cideciyan, A.V., Lewin, A.S., Hauswirth, W.W., Jacobson, S.G., and Aguirre, G.D. (2014). Gene augmentation for X-linked retinitis pigmentosa caused by mutations in RPGR. Cold Spring Harb. Perspect. Med. *5*, a017392.
17. Beltran, W.A., Cideciyan, A.V., Iwabe, S., Swider, M., Kosyk, M.S., McDaid, K., Martynyuk, I., Ying, G.S., Shaffer, J., Deng, W.T., et al. (2015). Successful arrest of photoreceptor and vision loss expands the therapeutic window of retinal gene therapy to later stages of disease. Proc. Natl. Acad. Sci. USA *112*, E5844–E5853.
18. Boye, S.E., Alexander, J.J., Boye, S.L., Witherspoon, C.D., Sandefer, K.J., Conlon, T.J., Erger, K., Sun, J., Ryals, R., Chiodo, V.A., et al. (2012). The human rhodopsin kinase promoter in an AAV5 vector confers rod- and cone-specific expression in the primate retina. Hum. Gene Ther. *23*, 1101–1115.
19. Beltran, W.A., Hammond, P., Acland, G.M., and Aguirre, G.D. (2006). A frameshift mutation in *RPGR* exon ORF15 causes photoreceptor degeneration and inner retina remodeling in a model of X-linked retinitis pigmentosa. Invest. Ophthalmol. Vis. Sci. *47*, 1669–1681.
20. Garcia, M.M., Ying, G.S., Cocores, C.A., Tanaka, J.C., and Komáromy, A.M. (2010). Evaluation of a behavioral method for objective vision testing and identification of achromatopsia in dogs. Am. J. Vet. Res. *71*, 97–102.
21. Wu, Z., Hiriyanna, S., Qian, H., Mookherjee, S., Campos, M.M., Gao, C., Fariss, R., Sieving, P.A., Li, T., Colosi, P., et al. (2015). A long-term efficacy study of gene replacement therapy for RPGR-associated retinal degeneration. Hum. Mol. Genet. *24*, 3956–3970.
22. Megaw, R.D., Soares, D.C., and Wright, A.F. (2015). RPGR: Its role in photoreceptor physiology, human disease, and future therapies. Exp. Eye Res. *138*, 32–41.
23. Zeiss, C.J., Acland, G.M., and Aguirre, G.D. (1999). Retinal pathology of canine X-linked progressive retinal atrophy, the locus homologue of RP3. Invest. Ophthalmol. Vis. Sci. *40*, 3292–3304.
24. Beltran, W.A., Acland, G.M., and Aguirre, G.D. (2009). Age-dependent disease expression determines remodeling of the retinal mosaic in carriers of RPGR exon ORF15 mutations. Invest. Ophthalmol. Vis. Sci. *50*, 3985–3995.
25. Beltran, W.A., Boye, S.L., Boye, S.E., Chiodo, V.A., Lewin, A.S., Hauswirth, W.W., and Aguirre, G.D. (2010). rAAV2/5 gene-targeting to rods:dose-dependent efficiency and complications associated with different promoters. Gene Ther. *17*, 1162–1174.
26. Hong, D.H., Pawlyk, B., Sokolov, M., Strissel, K.J., Yang, J., Tulloch, B., Wright, A.F., Arshavsky, V.Y., and Li, T. (2003). RPGR isoforms in photoreceptor connecting cilia and the transitional zone of motile cilia. Invest. Ophthalmol. Vis. Sci. *44*, 2413–2421.
27. Porrello, K., Bhat, S.P., and Bok, D. (1991). Detection of interphotoreceptor retinoid binding protein (IRBP) mRNA in human and cone-dominant squirrel retinas by in situ hybridization. J. Histochem. Cytochem. *39*, 171–176.
28. O'Brien, K.M., Schulte, D., and Hendrickson, A.E. (2003). Expression of photoreceptor-associated molecules during human fetal eye development. Mol. Vis. *9*, 401–409.

29. Boatright, J.H., Borst, D.E., Peoples, J.W., Bruno, J., Edwards, C.L., Si, J.S., and Nickerson, J.M. (1997). A major cis activator of the IRBP gene contains CRX-binding and Ret-1/PCE-I elements. Mol. Vis. *3*, 15.

30. Fong, S.L., and Fong, W.B. (1999). Elements regulating the transcription of human interstitial retinoid-binding protein (IRBP) gene in cultured retinoblastoma cells. Curr. Eye Res. *18*, 283–291.

31. Bobola, N., Briata, P., Ilengo, C., Rosatto, N., Craft, C., Corte, G., and Ravazzolo, R. (1999). OTX2 homeodomain protein binds a DNA element necessary for interphotoreceptor retinoid binding protein gene expression. Mech. Dev. *82*, 165–169.

32. Rath, M.F., Morin, F., Shi, Q., Klein, D.C., and Møller, M. (2007). Ontogenetic expression of the Otx2 and Crx homeobox genes in the retina of the rat. Exp. Eye Res. *85*, 65–73.

33. Vandenberghe, L.H., Bell, P., Maguire, A.M., Xiao, R., Hopkins, T.B., Grant, R., Bennett, J., and Wilson, J.M. (2013). AAV9 targets cone photoreceptors in the nonhuman primate retina. PLoS ONE *8*, e53463.

34. Ye, G.J., Budzynski, E., Sonnentag, P., Nork, T.M., Miller, P.E., Sharma, A.K., Ver Hoeve, J.N., Smith, L.M., Arndt, T., Calcedo, R., et al. (2016). Safety and biodistribution evaluation in cynomolgus macaques of rAAV2tYF-PR1.7-hCNGB3, a recombinant AAV vector for treatment of achromatopsia. Hum. Gene Ther. Clin. Dev. *27*, 37–48.

35. Lhériteau, E., Petit, L., Weber, M., Le Meur, G., Deschamps, J.Y., Libeau, L., Mendes-Madeira, A., Guihal, C., François, A., Guyon, R., et al. (2014). Successful gene therapy in the RPGRIP1-deficient dog: a large model of cone-rod dystrophy. Mol. Ther. *22*, 265–277.

36. Léveillard, T., Mohand-Saïd, S., Lorentz, O., Hicks, D., Fintz, A.C., Clérin, E., Simonutti, M., Forster, V., Cavusoglu, N., Chalmel, F., et al. (2004). Identification and characterization of rod-derived cone viability factor. Nat. Genet. *36*, 755–759.

37. Aguirre, G.D., Cideciyan, A.V., Boye, S.L., Iwabe, S., Dufour, V., Marinho, F.P., Downs, L.M., Hauswirth, W., Jacobson, S.G., and Beltran, W.A. (2016). AAV-mediated gene augmentation restores retinal function and vision in the canine model of NPHP5 Leber congenital amaurosis. Invest. Ophthalmol. Vis. Sci. *57*.

38. Liu, J., Espejo, A., Pan, W., and Ye, G.J. (2016). Rational design and cloning of a stable RPGR ORF15 cDNA encoding the full-length native RPGR protein. Mol. Ther. *24* (*Suppl 1*), S43–S44.

39. Zolotukhin, S., Potter, M., Zolotukhin, I., Sakai, Y., Loiler, S., Fraites, T.J., Jr., Chiodo, V.A., Phillipsberg, T., Muzyczka, N., Hauswirth, W.W., et al. (2002). Production and purification of serotype 1, 2, and 5 recombinant adeno-associated viral vectors. Methods *28*, 158–167.

40. Boye, S.E., Alexander, J.J., Witherspoon, C.D., Boye, S.L., Peterson, J.J., Clark, M.E., Sandefer, K.J., Girkin, C.A., Hauswirth, W.W., and Gamlin, P.D. (2016). Highly efficient delivery of adeno-associated viral vectors to the primate retina. Hum. Gene Ther. *27*, 580–597.

41. Pajusola, K., Gruchala, M., Joch, H., Lüscher, T.F., Ylä-Herttuala, S., and Büeler, H. (2002). Cell-type-specific characteristics modulate the transduction efficiency of adeno-associated virus type 2 and restrain infection of endothelial cells. J. Virol. *76*, 11530–11540.

42. Ryals, R.C., Boye, S.L., Dinculescu, A., Hauswirth, W.W., and Boye, S.E. (2011). Quantifying transduction efficiencies of unmodified and tyrosine capsid mutant AAV vectors in vitro using two ocular cell lines. Mol. Vis. *17*, 1090–1102.

43. Komáromy, A.M., Varner, S.E., de Juan, E., Acland, G.M., and Aguirre, G.D. (2006). Application of a new subretinal injection device in the dog. Cell Transplant. *15*, 511–519.

44. Beltran, W.A., Cideciyan, A.V., Guziewicz, K.E., Iwabe, S., Swider, M., Scott, E.M., Savina, S.V., Ruthel, G., Stefano, F., Zhang, L., et al. (2014). Canine retina has a primate fovea-like bouquet of cone photoreceptors which is affected by inherited macular degenerations. PLoS ONE *9*, e90390.

45. Zeger, S.L., and Liang, K.Y. (1986). Longitudinal data analysis for discrete and continuous outcomes. Biometrics *42*, 121–130.

YMTHE, Volume *25*

Supplemental Information

Optimization of Retinal Gene Therapy for X-Linked Retinitis Pigmentosa Due to *RPGR* Mutations

William A. Beltran, Artur V. Cideciyan, Shannon E. Boye, Guo-Jie Ye, Simone Iwabe, Valerie L. Dufour, Luis Felipe Marinho, Malgorzata Swider, Mychajlo S. Kosyk, Jin Sha, Sanford L. Boye, James J. Peterson, C. Douglas Witherspoon, John J. Alexander, Gui-Shuang Ying, Mark S. Shearman, Jeffrey D. Chulay, William W. Hauswirth, Paul D. Gamlin, Samuel G. Jacobson, and Gustavo D. Aguirre

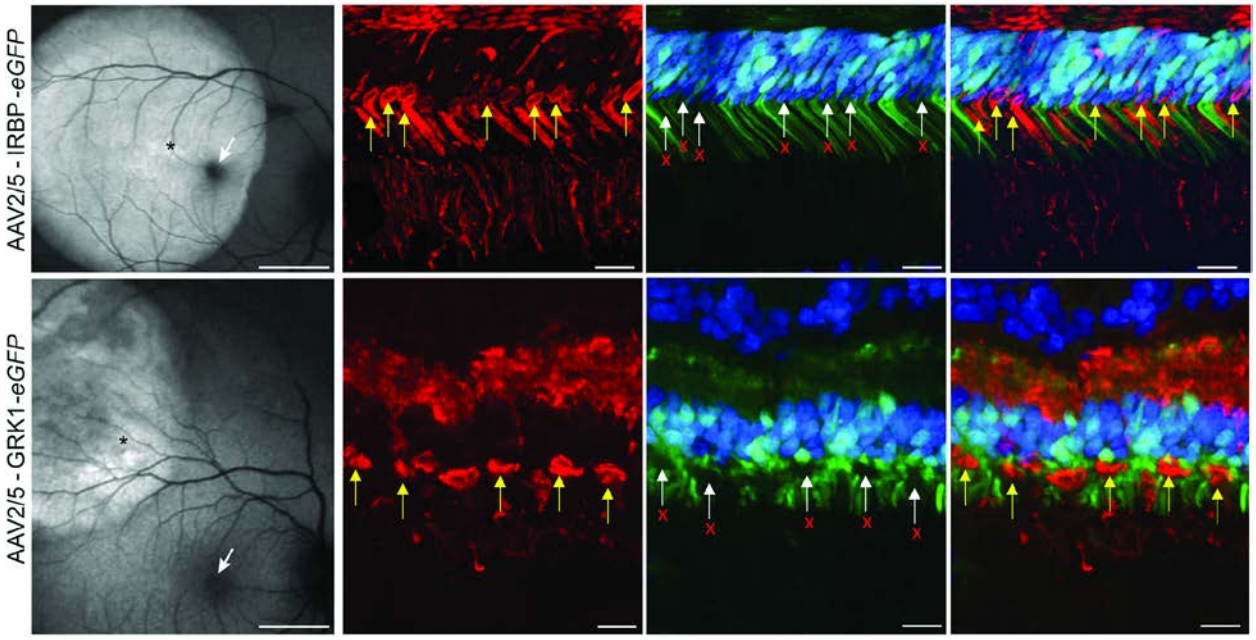

Figure S1: GFP expression in macaque photoreceptors 8 weeks post-subretinal injection with low titers of AAV2/5 using IRBP or GRK1 promoters. (**Upper row**) Expression of eGFP was detected in life within the bleb area but not in the foveal region (white arrow) of the right eye of NHP #080113 injected with 100 µL of AAV2/5-IRBP-*eGFP* at a titer of 3 x 10^{11} vg/mL.. Retinal cross sections within the treated area (depicted by an asterisk on the cSLO fundus image) were stained with an antibody against cone arrestin (red) and counterstained with DAPI (blue). Images reveal GFP expression (green) in rod, but not cone photoreceptors (yellow arrows), as evidenced by the lack of fluorescence in cone-arrestin-positive cells (white arrows with red "X" denote GFP- negative cone cell bodies). (**Lower row**) Expression of eGFP was detected in life within the superior temporal region of the left retina (displayed as equivalent right eye) of NHP#AT459 injected with 100 µL of AAV2/5-GRK1-*eGFP* at a titer of 1.5 x 10^{11} vg/mL. White arrow points to the fovea. Retinal cross sections within the treated area (depicted by an asterisk on the cSLO fundus image) reveal GFP expression within rods, but not cone photoreceptors of the peripheral retina. Cone arrestin- positive cones (yellow arrows) in this retina did not express GFP (white arrows with red "X" denote GFP-negative cone cell bodies). Scale bars (cSLO images) = 10 degrees; scale bars (immunolabeled sections) = 17 µm.

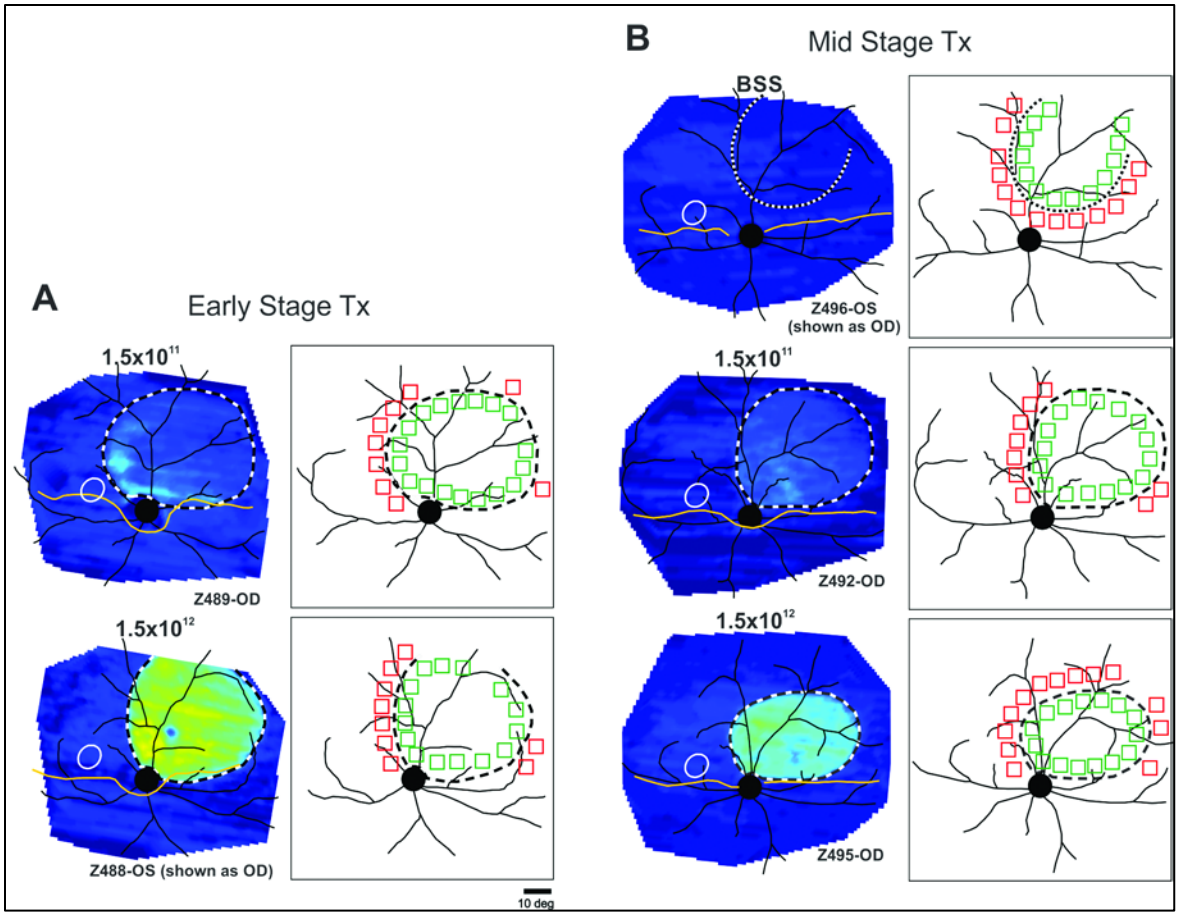

Figure S2: Retinal loci selected for quantitative evaluation of ONL thickness rescue after intervention at early (A) and mid (B) stage disease. Pseudocolor maps of ONL thickness topography, left, are duplicated from Figure 3. Outermost treatment boundary estimates are either based on fundus photographs of the bleb taken at the time of the injection (dotted lines) or, if visible, demarcations apparent on infrared imaging at the time of scanning (dashed lines). Schematics, right, show loci selected inside (green) or outside (red) the outermost treatment boundary for quantitative evaluation.

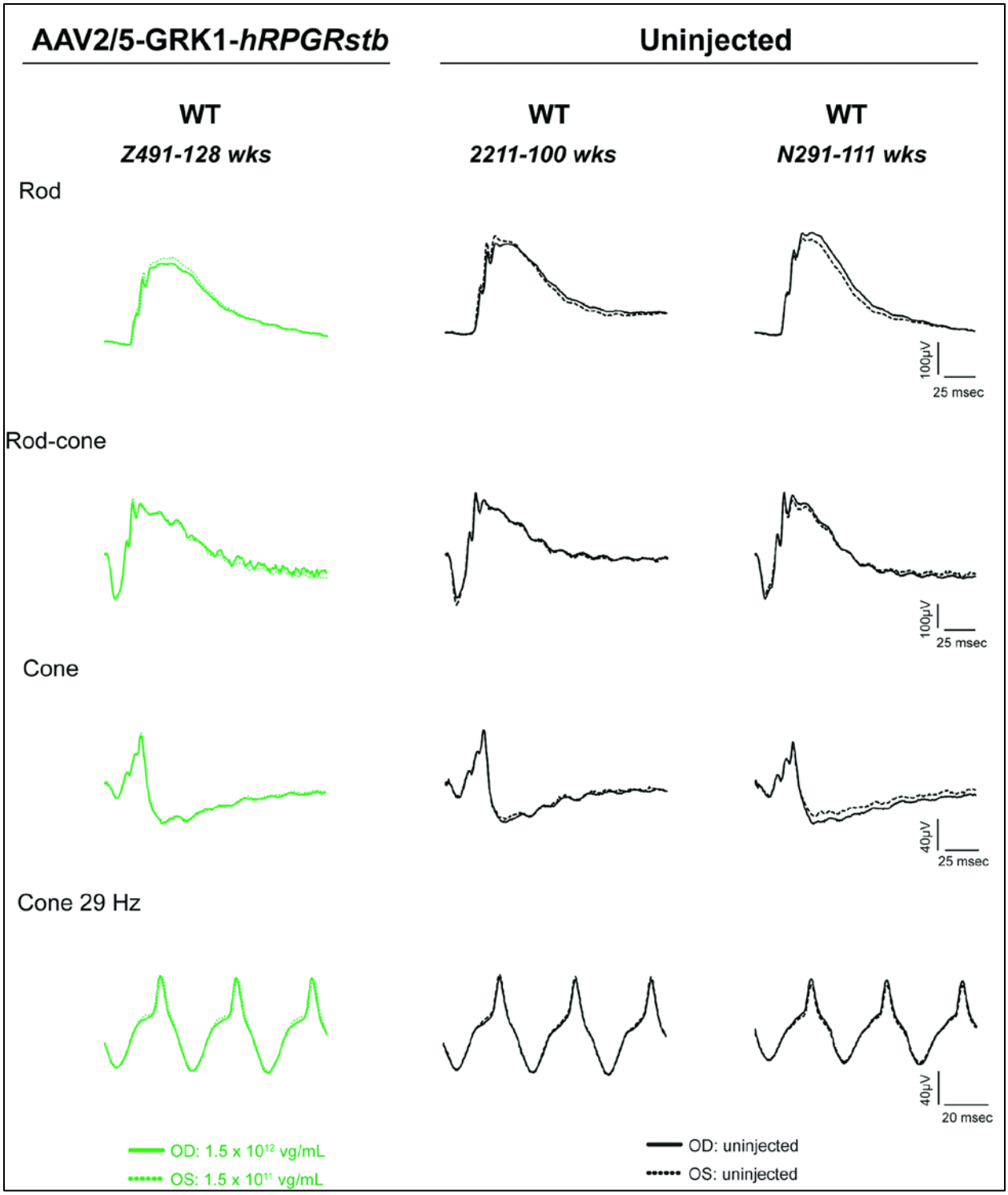

Figure S3: Long-term assessment of retinal function after subretinal injection with AAV2/5-GRK1-*hRPGRstb* in WT dog. ERG traces (green) of rod (-1.74 log cd.s.m^{-2}), mixed rod-cone (1.01 log cd.s.m^{-2}) responses recorded under dark-adaptation, and cone (1.01 log cd.s.m^{-2}) responses to single stimuli or 29 Hz cone flicker (0.76 log cd.s.m^{-2}) recorded under light adaptation at 128 weeks of age in a WT dog treated at 5 weeks of age with AAV2/5-GRK1-*hRPGRstb* at 1.5x10^{11} vg/mL in the right eye (OD) and at 1.5x10^{12} vg/mL in the left eye (OS). Similar ERG recordings (black traces) are shown from 4 uninjected eyes of two WT dogs.

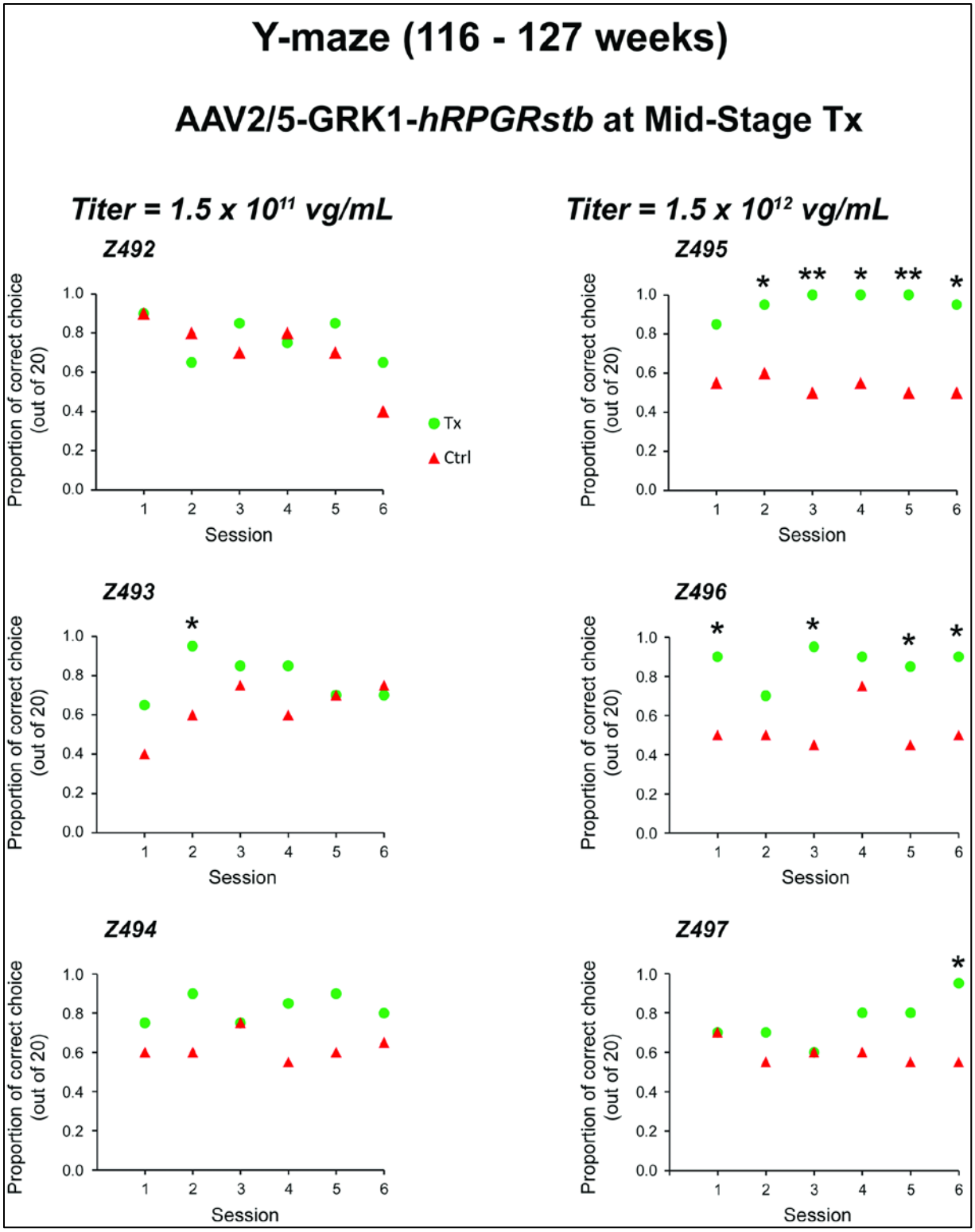

Figure S4: Individual results of visually-guided behavior in a forced 2-choice Y maze. RPGR mutant dogs were treated at 12 weeks of age with AAV2/5-GRK1-*hRPGRstb* at either $1.5x10^{11}$ or $1.5x10^{12}$ vg/mL titers and tested during 6 sessions between 116-127 weeks of age. Tx: treated; Ctrl: contralateral BSS injected. *: $p<0.05$; **: $p<0.001$ from Fisher exact test between treated and contralateral eyes.

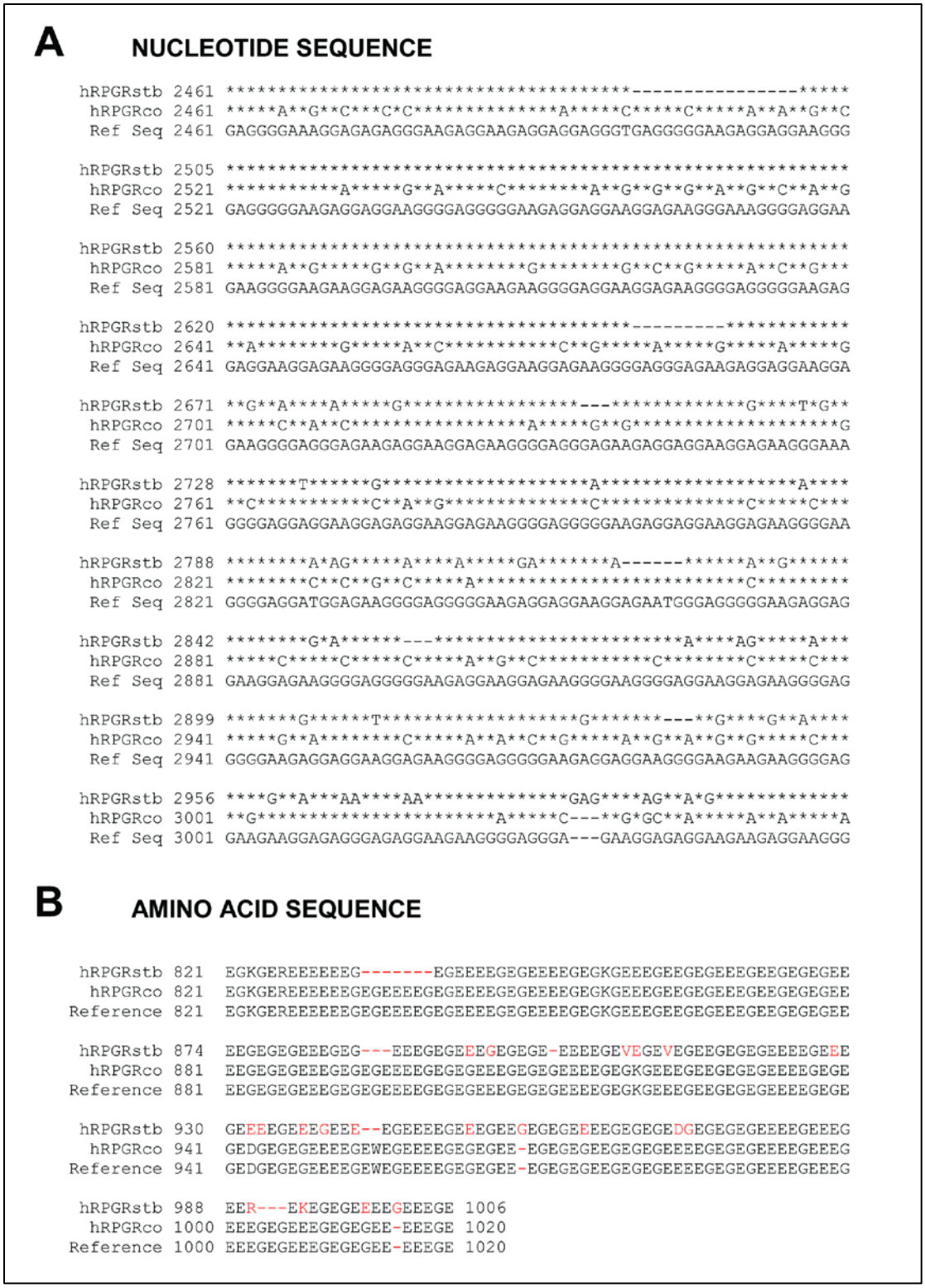

Figure S5: Nucleotide and amino acid sequence alignments of the ORF15 domains of hRPGRstb, hRPGRco and the GenBank hRPGR reference sequence (accession number: NM_001034853.1). Asterisks(*) indicate nucleotide or amino acid that is identical to the reference sequence, and dashes (-) indicate nucleotide or amino acid deletion. Complete nucleotide sequences of hRPGRco is available in GenBank (accession number: KY293401).

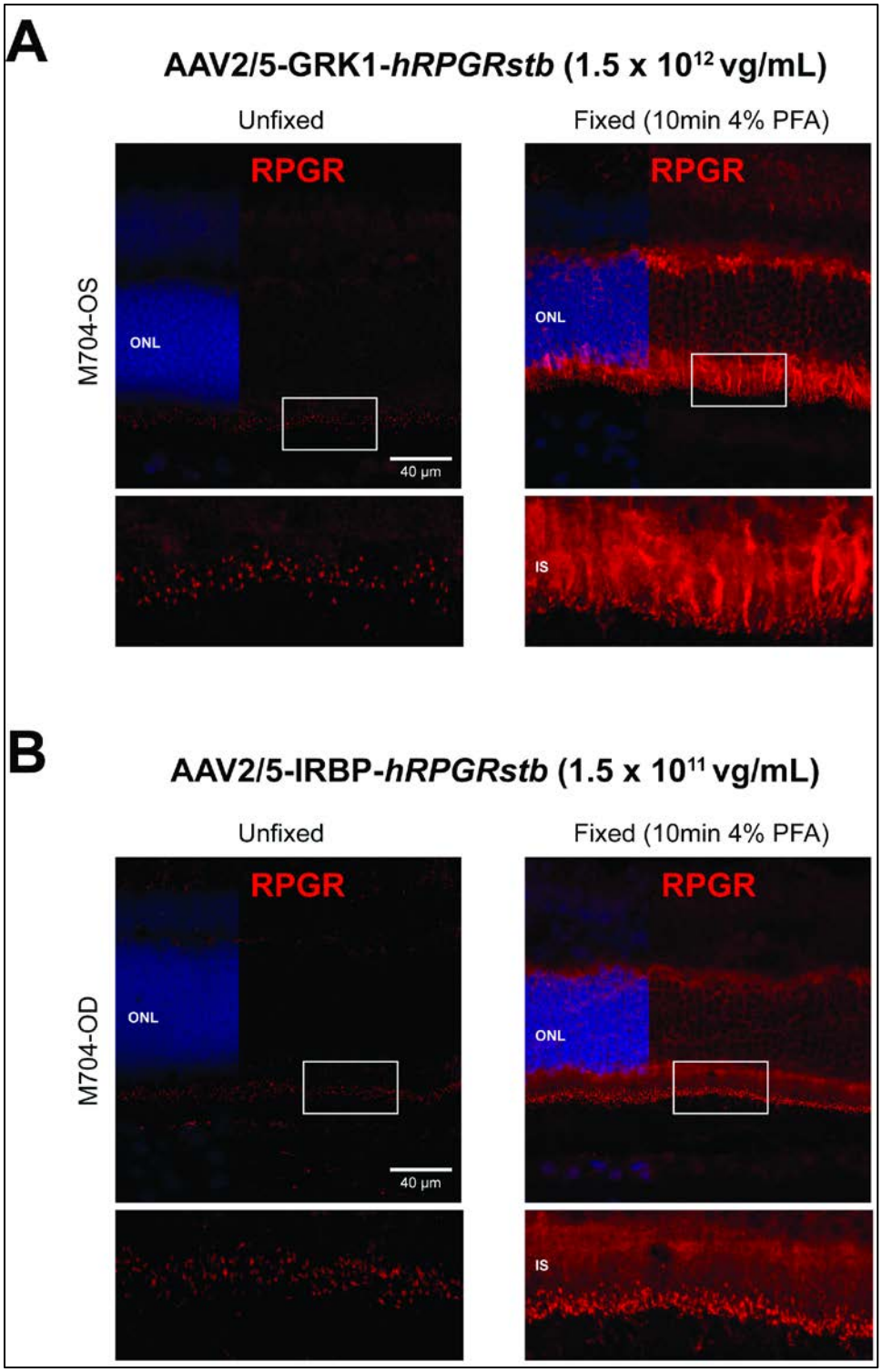

Figure S6: Influence of tissue fixation on RPGR transgene immunolabeling. (**A**) RPGR immunolabeling in the treated area of a WT retina injected with AAV2/5-GRK1-*hRPGRstb* at $1.5x10^{12}$ vg/mL in left eye (OS), or (**B**) injected in the right eye (OD) with AAV2/5-IRBP-*hRPGRstb* at $1.5x10^{11}$ vg/mL. Left panels show labeling in an unfixed section, right panels show labeling in a section from the same eyes fixed for 10 min in 4% paraformaldehyde. Note that the RPGR antibody used recognizes the human transgene product, but not endogenous canine RPGR.

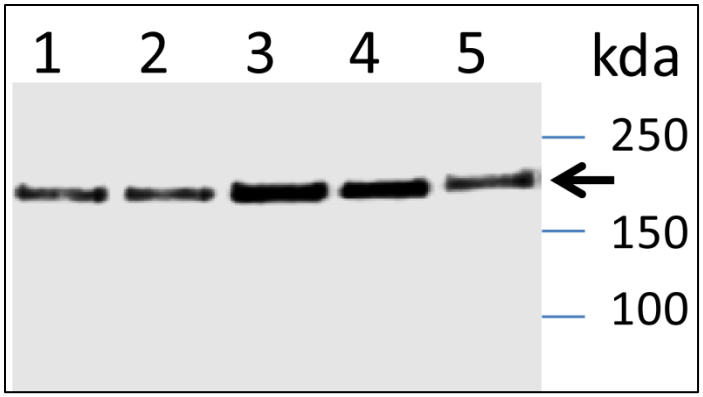

Figure S7: Western blot showing expressed hRPGR protein in HEK293 cells with a hRPGR specific antibody. Cell lysate of HEK293 cells transfected with pTR-CBA-hRPGRco (Lanes 1 and 2: 0.15 µg total protein); infected with AAV-CBA-hRPGRco (Lanes 3 and 4: 0.3 µg of total protein); infected with AAV-GRK1-hRPGRco (Lane 5, 10 µg of total protein) , adjusted to a final total protein of 10 µg/lane by adding normal HEK293 cell lysate were subjected to SDS-PAGE followed by Western blot with a mouse monoclonal anti-hRPGR antibody (mAB-C3, AGTC customer made). A hRPGR specific protein band close to 200 kda was detected in cells transfected with the AAV production plasmid (with CBA promoter), or infected with AAV-hRPGRco vectors containing either CBA or GRK1 promoter. As expected, the expression level of hRPGR from AAV-hRPGR driven by photoreceptor specific GRK1 promoter (Lane 5) was much lower than that from plasmid or AAV-hRPGR driven by the ubiquitous CBA promoter. (Lanes 1 to 4).

Table S1. Summary of the experimental procedures performed in NHPs.

Animal ID	Eye	Age (wks)		Duration (wks)	Treatment			Analysis	Studies	Figure
		Begin	End		AAV2/5 construct	Titer (vg/mL)/ *volume (μL)*	Dose (vg/eye)			
M. mulatta										
080113	OD	208	216	8	IRBP-e*GFP*	$3x10^{11}$/*100*	$3 x10^{10}$	cSLO; IHC	Promoter activity/ titer comparison	Fig. S1
080113	OS	208	216	8	IRBP-e*GFP*	$3x10^{11}$/*100*	$3 x10^{10}$	cSLO; IHC	Promoter activity/ titer comparison	
090365	OD	214	222	8	IRBP-e*GFP*	$1x10^{12}$/*100*	$10 x10^{10}$	cSLO; IHC	Promoter activity/ titer comparison	Fig. 2B, B1, B2, B3
090365	OS	214	222	8	IRBP-e*GFP*	$1x10^{12}$/*100*	$10 x10^{10}$	cSLO; IHC	Promoter activity/ titer comparison	Fig. 2A, A1, A2, A3, A4, A5, A6
M. fascicularis										
AT459	OD	680	690	10	GRK1-e*GFP*	$1.5x10^{11}$/*50*	$0.75 x 10^{10}$	cSLO; IHC	Promoter activity/ titer comparison	
AT459	OS	680	690	10	GRK1-e*GFP*	$1.5x10^{11}$/*100*	$1.5 x 10^{10}$	cSLO; IHC	Promoter activity/ titer comparison	Fig. S1
AV136	OD	673	683	10	GRK1-e*GFP*	$1.5x10^{12}$/*90*	$13.5 x 10^{10}$	cSLO; IHC	Promoter activity/ titer comparison	Fig. 2C, C1, C2, C3
AV136	OS	673	683	10	GRK1-e*GFP*	$1.5x10^{12}$/*100*	$15 x 10^{10}$	cSLO; IHC	Promoter activity/ titer comparison	Fig. 2D, D1, D2, D3

OD: right eye; OS: left eye; IRBP: human interphotoreceptor retinoid binding protein (promoter); GRK1: human rhodopsin kinase-1 (promoter); eGFP: humanized enhanced green fluorescent protein; cSLO: confocal scanning laser ophthalmoscopy; IHC: immunohistochemistry.

Table S2. Summary of the experimental procedures performed in dogs.

Studies	Animal ID	Eye	Age (wks)		Duration (wks)	Treatment			Analysis	Figure
			Begin	Last exam		AAV2/5 construct	Titer (vg/mL)/ *volume (μL)*	Dose (vg/eye)		
***RPGR* mutant**										
Early-stage Tx										
	Z488	OD	5	102	97	GRK1-*hRPGRstb*	1.5×10^{11}/*100*	1.5×10^{10}	cSLO/OCT	Fig. 3D
	Z488	OS	5	102	97	GRK1-*hRPGRstb*	1.5×10^{12}/*70*	10.5×10^{10}	cSLO/OCT	Fig. 3B,D; S2A
	Z489	OD	5	102	97	GRK1-*hRPGRstb*	1.5×10^{11}/*70*	1.05×10^{10}	cSLO/OCT	Fig. 3B,D; S2A
	Z489	OS	5	102	97	GRK1-*hRPGRstb*	1.5×10^{12}/*70*	10.5×10^{10}	cSLO/OCT	Fig. 3D
Mid stage-Tx, titer comparison										
	Z492	OD	12	105	93	GRK1-*hRPGRstb*	1.5×10^{11}/*150*	2.25×10^{10}	cSLO/OCT; ERG; VB	Fig. 3C,D; 4B; 5; S2B; S4
	Z492	OS	12	105	93	BSS	/		cSLO/OCT; ERG; VB	Fig. 3D; 4B; 5; S4
	Z493	OD	12	105	93	GRK1-*hRPGRstb*	1.5×10^{11}/*150*	2.25×10^{10}	cSLO/OCT; ERG; VB	Fig. 3D; 4A,B; 5; S4
	Z493	OS	12	105	93	BSS	/		cSLO/OCT; ERG; VB	Fig. 3D; 4A,B; 5; S4
	Z494	OD	12	105	93	GRK1-*hRPGRstb*	1.5×10^{11}/*150*	2.25×10^{10}	cSLO/OCT; ERG; VB	Fig. 3D; 4B; 5; S4
	Z494	OS	12	105	93	BSS	/		cSLO/OCT; ERG; VB	Fig. 3D; 4B; 5; S4
	Z495	OD	12	105	93	GRK1-*hRPGRstb*	1.5×10^{12}/*150*	22.5×10^{10}	cSLO/OCT; ERG; VB	Fig. 3C,D; 4D; 5; S2B; S4
	Z495	OS	12	105	93	BSS	/		cSLO/OCT; ERG; VB	Fig. 3D; 4D; 5; S4
	Z496	OD	12	105	93	GRK1-*hRPGRstb*	1.5×10^{12}/*150*	22.5×10^{10}	cSLO/OCT; ERG; VB	Fig. 3D; 4D; 5; S4
	Z496	OS	12	105	93	BSS	/		cSLO/OCT; ERG; VB	Fig. 3C,D; 4D; 5; S2B; S4
	Z497	OD	12	106	94	GRK1-*hRPGRstb*	1.5×10^{12}/*150*	22.5×10^{10}	cSLO/OCT; ERG; VB	Fig. 3D; 4C,D; 5; S4
	Z497	OS	12	106	94	BSS	/		cSLO/OCT; ERG; VB	Fig. 3D; 4C,D; 5; S4
hRPGR transgene comparison										
	Z517	OD	6.1	18	11.9	GRK1-*hRPGRco*	7.2×10^{11}/*70*	5.04×10^{10}	cSLO/OCT; IHC	Fig. 6C,D
	Z517	OS	6.1	18	11.9	GRK1-*hRPGRstb*	7.2×10^{11}/*70*	5.04×10^{10}	cSLO/OCT; IHC	Fig. 6C,D
	Z521	OD	6.1	18	11.9	GRK1-*hRPGRco*	7.2×10^{11}/*70*	5.04×10^{10}	cSLO/OCT; IHC	Fig. 6B,C,D
	Z521	OS	6.1	18	11.9	Uninjected			cSLO/OCT; IHC	Fig. 6B,C,D
	Z522	OD	6.1	18	11.9	GRK1-*hRPGRstb*	7.2×10^{11}/*70*	5.04×10^{10}	cSLO/OCT; IHC	Fig. 6A,C,D
	Z522	OS	6.1	18	11.9	Uninjected			cSLO/OCT; IHC	Fig. 6A,C,D
	Z524	OD	5.7	23.5	17.8	GRK1-*hRPGRco*	7.2×10^{11}/*70*	5.04×10^{10}	cSLO/OCT; IHC	Fig. 6C,D
	Z524	OS	5.7	23.5	17.8	Uninjected			cSLO/OCT; IHC	Fig. 6C,D
	Z525	OD	5.7	23.5	17.8	GRK1-*hRPGRstb*	7.2×10^{11}/*70*	5.04×10^{10}	cSLO/OCT; IHC	Fig. 6C,D
	Z525	OS	5.7	23.5	17.8	Uninjected			cSLO/OCT; IHC	Fig. 6C,D
	Z526	OD	5.7	23.5	17.8	GRK1-*hRPGRco*	7.2×10^{11}/*70*	5.04×10^{10}	cSLO/OCT; IHC	Fig. 6C,D; 7
	Z526	OS	5.7	23.5	17.8	GRK1-*hRPGRstb*	7.2×10^{11}/*70*	5.04×10^{10}	cSLO/OCT; IHC	Fig. 6C,D; 7
	Z528	OD	5.7	23.5	17.8	GRK1-*hRPGRco*	7.2×10^{11}/*70*	5.04×10^{10}	cSLO/OCT; IHC	Fig. 6C,D
	Z528	OS	5.7	23.5	17.8	Uninjected			cSLO/OCT; IHC	Fig. 6C,D
***WT* (normal)**										
Short-term safety										
	Z487	OD	14	27	13	GRK1-*hRPGRstb*	1.5×10^{12}/*150*	22.5×10^{10}	cSLO/OCT	
	Z487	OS	14	27	13	GRK1-*hRPGRstb*	1.5×10^{11}/*150*	2.25×10^{10}	cSLO/OCT	
Long-term safety										
	Z490	OD	5	102	97	GRK1-*hRPGRstb*	1.5×10^{11}/*70*	1.05×10^{10}	cSLO/OCT	Fig. 3D
	Z490	OS	5	102	97	GRK1-*hRPGRstb*	1.5×10^{12}/*70*	10.5×10^{10}	cSLO/OCT	Fig. 3D

	Z491	OD	5	102	97	GRK1-*hRPGRstb*	1.5 x 10^{11}/*70*	1.05 x 10^{10}	cSLO/OCT; ERG	Fig. 3D; S3
	Z491	OS	5	102	97	GRK1-*hRPGRstb*	1.5 x 10^{12}/*70*	10.5 x 10^{10}	cSLO/OCT; ERG	Fig. 3D; S3
RPGR IHC with and without fixation										
	M704	OS	152	160	8	GRK1-*hRPGRstb*	1.5 x 10^{12}/*150*	22.5 x 10^{10}	cSLO/OCT; IHC	Fig. S6A
	M704	OD	152	160	8	IRBP-*hRPGRstb*	1.5 x 10^{11}/*150*	2.25 x 10^{10}	cSLO/OCT; IHC	Fig. S6B
WT control										
	AS340	OD	16	/	/	Uninjected			cSLO/OCT	Fig. 3A,D
	D204	OD	22	/	/	Uninjected			cSLO/OCT	Fig. 3A,D
	WBT60	OD	35	/	/	Uninjected			cSLO/OCT	Fig. 3A,D
	CGBCAN	OD	37	/	/	Uninjected			cSLO/OCT	Fig. 3A,D
	CGBCAN	OS	37	/	/	Uninjected			cSLO/OCT	Fig. 3A,D
	CGBCDI	OD	37	/	/	Uninjected			cSLO/OCT	Fig. 3A,D
	CGBCDI	OS	37	/	/	Uninjected			cSLO/OCT	Fig. 3A,D
	CGBCGS	OD	37	/	/	Uninjected			cSLO/OCT	Fig. 3A,D
	CGBCGS	OS	37	/	/	Uninjected			cSLO/OCT	Fig. 3A,D
	D340	OD	43	/	/	Uninjected			cSLO/OCT	Fig. 3A,D
	N284	OS	140	/	/	Uninjected			cSLO/OCT	Fig. 3A,D
	N269	OS	198	/	/	Uninjected			cSLO/OCT	Fig. 3A,D
	2211	OD	100	/	/	Uninjected			ERG	Fig. S3
	2211	OS	100	/	/	Uninjected			ERG	Fig. S3
	N291	OD	111	/	/	Uninjected			ERG	Fig. S3
	N291	OS	111	/	/	Uninjected			ERG	Fig. S3

OD: right eye; OS: left eye; IRBP: human interphotoreceptor binding protein (promoter); GRK1: human rhodopsin kinase-1 (promoter); *hRPGRstb*: stabilized human *RPGR* cDNA; *hRPGRco*: stabilized codon-optimized human *RPGR* cDNA; cSLO: confocal scanning laser ophthalmoscopy; OCT: optical coherence tomography; ERG: electroretinography; IHC: immunohistochemistry; VB: visual behavior testing (Y maze and obstacle avoidance course).

Table S3. Comparison of AAV2/5-GRK1-*hRPGRstb* treatment effect on ERG a-wave amplitude between low titer (1.5×10^{11} vg/mL) and high titer (1.5×10^{12} vg/mL) groups

Light Intensity (log cd.s/m^2)	Mean (SD) difference between treated eyes and control eyes (μV)		
	Low titer group	High titer group	P-value*
-3.74	0.00(0.00)	0.00(0.00)	-
-3.25	0.00(0.00)	0.00(0.00)	-
-2.74	0.00(0.00)	0.00(0.00)	-
-2.24	0.00(0.00)	0.00(0.00)	-
-1.74	0.00(0.00)	0.00(0.00)	-
-1.24	1.15(1.43)	4.44(2.48)	0.12
-0.74	1.90(2.87)	7.55(4.88)	0.16
-0.25	1.29(1.17)	12.11(4.85)	**0.02**
0.26	1.75(1.52)	12.35(5.76)	**0.04**
0.51	1.43(1.51)	15.14(8.37)	**0.049**

*From two-sample t-test.

Table S4. Comparison of AAV2/5-GRK1-*hRPGRstb* treatment effect on ERG b-wave amplitude between low titer (1.5×10^{11} vg/mL) and high titer (1.5×10^{12} vg/mL) groups.

Light Intensity (log cd.s/m^2)	Mean (SD) in difference between treated eyes and control eyes (μV)		
	Low titer group	High titer group	P-value*
-3.74	0.00 (0.00)	2.36 (4.10)	0.42
-3.25	3.86 (6.69)	18.03 (8.68)	0.09
-2.74	5.44 (9.42)	34.29 (15.73)	0.053
-2.24	7.16 (12.41)	55.31 (25.52)	**0.04**
-1.74	11.08 (9.33)	64.95 (29.82)	**0.04**
-1.24	14.64 (8.72)	67.81 (32.33)	0.051
-0.74	14.23 (6.14)	77.43 (37.35)	**0.04**
-0.25	14.40 (8.06)	80.92 (40.55)	**0.0495**
0.26	14.94 (7.31)	80.15 (35.21)	**0.03**
0.51	14.62 (10.17)	84.82 (36.44)	**0.03**

*From two-sample t-test.

Table S5. Comparison of AAV2/5-GRK1-*hRPGRstb* treatment effect on photopic ERG b-wave amplitude between low titer (1.5×10^{11} vg/mL) and high titer (1.5×10^{12} vg/mL) groups.

Light Intensity (log cd.s/m^2)	Mean (SD) in difference between treated eyes and control eyes (μV)		
	Low titer group	High titer group	P-value*
-2.74	0.00 (0.00)	0.00 (0.00)	-
-2.24	0.00 (0.00)	0.00 (0.00)	-
-1.74	0.00 (0.00)	0.00 (0.00)	-
-1.24	0.67 (1.15)	1.82 (1.61)	0.37
-0.74	3.43 (0.88)	5.45 (1.97)	0.18
-0.25	4.91 (2.19)	10.20 (7.11)	0.29
0.26	6.37 (0.63)	16.79 (8.40)	0.16
0.51	6.27 (2.21)	15.86 (7.45)	0.10

*From two-sample t-test.

Table S6. Comparison of AAV2/5-GRK1-*hRPGRstb* treatment effect on photopic 29 Hz flicker amplitude between low titer (1.5×10^{11} vg/mL) and high titer (1.5×10^{12} vg/mL) groups.

Light Intensity (log cd.s/m^2)	Mean (SD) in difference between treated eyes and control eyes (μV)		
	Low titer group	High titer group	P-value*
-2.74	0.00 (0.00)	0.00 (0.00)	-
-2.24	0.00 (0.00)	0.00 (0.00)	-
-1.74	0.00 (0.00)	0.00 (0.00)	-
-1.24	0.27 (0.46)	0.82 (1.41)	0.56
-0.74	3.67 (0.32)	4.80 (2.06)	0.44
-0.25	3.30 (2.59)	10.84 (5.59)	0.10
0.26	5.88 (1.55)	14.87 (12.05)	0.33

*From two-sample t-test.